Probing the space-time structure of quark and gluon transport in proton-nucleus collisions at collider energies

K. Geiger*

Institute for Theoretical Physics, University of California, Santa Barbara, California 93106
and School of Physics and Astronomy, University of Minnesota, Minneapolis, Minnesota 55455

(Received 18 November 1993)

The $\sqrt{s}$ and A dependence of ultrarelativistic pA collisions for energies corresponding to future collider experiments at RHIC and LHC is studied with focus on medium effects that affect the parton evolution in nuclear matter. Within the parton cascade model the saturation of the parton densities due to unitarity conservation, the self-contained balance of parton emission and fusion processes, and the mechanism of dynamical screening of long range interactions are analyzed. The resulting inclusive spectra and properties of secondary hadrons are discussed in order to extract aspects of "QCD in medium" from collider experiments.

I. INTRODUCTION

The relativistic collider facilities, the BNL relativistic heavy ion collider (RHIC) under construction, and the Large Hadron Collider (LHC) close to approval, will for the first time provide the opportunity to systematically study the physics of hot and ultradense matter in hadron-nucleus (pA) and nucleus-nucleus (AB) collisions at energies that are orders of magnitude larger than at current accelerators. The variations in collider energies and nuclear beams allow a careful analysis of the dependence of multiparticle production on the center-of-mass energy $\sqrt{s}$ and mass number A. By comparing pA and AA reactions involving very heavy nuclei, a sensitive examination of the particle spectra with respect to the kinematic variables rapidity and transverse momentum may be capable of distinguishing basic hadronic effects that dominate the dynamics in pA collisions [1], from a quark-gluon plasma (QGP) formation [2] predicted to occur in heavy ion AA collisions [3]. To gain insight into the underlying hadronic processes, one has to study collisions that are not expected to lead to a QGP formation.

Here lies the first motivation of this paper, namely to focus on pA collisions and to investigate the $\sqrt{s}$ and A dependences of global observables using the *parton cascade model* (PCM) [4,5] that is founded on "improved QCD perturbation theory" embedded in the framework of kinetic theory. During the last year broad confidence has grown that for ultrarelativistic energies at RHIC and beyond, perturbative QCD provides a good basis for the description of the global reaction dynamics and not just for rare fluctuations. Under this premise the PCM has been used to study primarily AA collisions, addressing issues of multiparticle production, thermal and chemi-

cal equilibration, dilepton, and flavor production [6]. To elucidate how the physics may change when proceeding from pp to AA collisions, I will turn here to pA collisions within this specific model framework, and study the A dependence by varying A from 1 to 238, for two fixed beam momenta per nucleon, $P = 100$ GeV and $P = 3000$ GeV, in correspondence to the highest available heavy ion beam energies at RHIC, respectively LHC [7].

The second motivation to study pA reactions arises from more theoretical grounds, but is also of great importance for the experimental concepts concerning detector design etc. Up to now, there is considerable theoretical uncertainty in perturbative QCD predictions for global observables in heavy ion collisions at high energies, such as particle multiplicities and transverse energy production, although hadron-hadron collisions at these energies are very well understood nowadays [8]. The discrepancy between a very accurate description of pp $(p\bar{p})$ data and rather crude predictions for AA collisions is due to the current lack of better knowledge about the details of important nuclear and dense medium effects. It is neither surprising, nor satisfying, that numerical simulations with QCD based Monte Carlo models such as HIJING [9], DTUJET [10], or the PCM, agree very well in describing pp collisions at collider energies, but differ in their predictions, e.g., charged particle multiplicities in heavy ion AA collisions, by a factor of 2 or more.

Recently considerable progress has been made in a better understanding of the space-time structure of quark and gluon interactions at collider energies [11]; however, one is still far from a complete and detailed picture. The qualitative picture that emerges [12] is that, at least for RHIC energies and beyond, most of the entropy and transverse energy is produced very rapidly after the moment of nuclear contact, by very frequent, mostly inelastic parton interactions that involve momentum transfers of only a few GeV. It is realized that these so-called "semihard" processes [13,14] play the major role for the nuclear dynamics at collider energies as has been dis-

---

*Present address: CERN TH-Division, CH-1211 Geneva 23, Switzerland.

cussed in a number of earlier works [15–22]. They cannot be considered as isolated rare events, but are embedded in complicated multiple cascade-type processes. At the same time it is found [23] that color correlations among the initial partons must disappear so rapidly that the long range color field effectively disappears. Thus the short range character of the interactions implies that perturbative QCD can and must be used, and that for example the string picture does not apply anymore. In trying to gain a more quantitative knowledge about the microscopic parton dynamics, the most urgent questions concern the magnitude of nuclear shadowing effects, the role of color screening and color diffusion, the impact of the Landau-Pomeranchuk-Migdal effect, and the influence of the characteristic interaction times of parton scatterings, as well as the formation times for gluons emitted in bremsstrahlung processes.

One of the most controversial issues is the huge entropy production due to very intense gluon multiplication in nuclear matter [12,24] that is triggered by frequent parton collisions. In free space where the parton evolution is determined unambiguously by squares of S-matrix elements that involve integration over all space and time, from the time of production to the infinite future. Here one deals with well-defined asymptotic states and the time scales of the intermediate interactions are irrelevant. However, inside nuclear matter the partons are likely to undergo multiple interactions with the nuclear medium, so that the integration cannot be extended before the previous interaction point, or beyond the current point of time. Within this context the essential questions are: (i) is there an upper limit on the amount of gluon multiplication imposed by unitarity, (ii) how do the reverse processes of parton fusion affect the evolution, (iii) what is the effect of Debye screening of long range interactions in dense nuclear matter for nonequilibrium systems, and (iv) what are the modifications of the scattering and emission probabilities subject to finite time scales and short mean free paths. In this paper I will address specifically these questions. I aim to elucidate the importance of a self-consistent dynamical parton evolution in both space-time and momentum space and will study how the final hadron spectra can reflect the structure of parton interactions in the nuclear environment of high energy collisions with nuclei. The results of the calculations generally show that for pA collisions involving light and intermediate heavy nuclei these medium effects have moderate impact, but for reactions with heavy nuclei the effects become essential and give rise to a saturating behavior for particle production, energy deposition, nuclear stopping power, etc. For quick reading, an itemized summary of the results and implications is given in the conclusions at the end of this paper.

I believe that a systematic study of pA collisions at the same energies is essential to gain insight into the structure of the mentioned medium effects, since these are absent in pp collisions, but become increasingly prominent in pA collisions, and are of major importance in AA reactions. Hence, by increasing the target mass A and the collider beam energy $\sqrt{s}$ in pA collisions, one may probe nuclear matter as a function of its density

and study the gradually growing impact of medium and nuclear effects by comparing to pp collisions. Once the physics of "QCD in medium" is better understood, the mechanisms of quark-gluon plasma formation and related collective phenomena in heavy ion collisions can be disentangled from the basic hadronic effects.

The paper is organized as follows. In Sec. II the essential aspects of the "improved parton picture" are recalled with specific focus on ultrarelativistic hadron-nucleus collisions and subsequently the framework of the PCM is briefly summarized. Section III is devoted to the space-time structure of these reactions on the parton level, namely, the effects of the saturation of the parton densities due to unitarity conservation, the balance of emission and fusion processes, and the role of dynamical screening of long range interactions. In Sec. IV I will show how properties of produced secondary hadrons reflect the characteristics of the preceding parton evolution, so that experimental analyses of the inclusive hadron spectra, the average transverse momentum dependence, and transverse energy production may be able to extract some of the new aspects of "QCD in medium." A summary and conclusion is given in Sec. V.

II. SPACE-TIME DESCRIPTION OF HIGH-ENERGY pA COLLISIONS

A. The parton picture and kinematics

It is now widely accepted that nuclear collisions at sufficiently high energies can well be described within the parton picture of hadronic interactions. For comprehensive reviews of the "old" parton model I refer to Refs. [25–28]. Its modern version [29–32] is based on renormalization group improved perturbative QCD [33] and provides a firmly established foundation which supports the point of view that the major part of the hadronic cross section, entropy, and transverse energy production, arise from so-called semihard processes [13,14] involving very frequent production of minijets [15,19] with a typical momentum transfer of a few GeV. The applicability of this picture is controlled by the smallness of the QCD coupling strength $\alpha_s(Q^2)$, implying $Q^2 > 1$ GeV^2, and thus relies on the short distance character of parton interactions for which long range forces and color correlations are irrelevant [23]. This condition is expected to be well fulfilled in nuclear collisions at the future colliders RHIC and LHC—at least during the early stage of the reactions.

In order to apply the parton picture to pA collisions one has to go into a frame where both the projectile proton and the target nucleus are moving very fast, so that both the proton and the nucleons in the nucleus can be resolved into individual partons. The visualization of a nucleon as an instantaneous distribution of partons at any time requires probing the nucleon over a time duration and spatial distance small on the scale of internal motions of the partons. This condition is fulfilled in any frame of reference in which the nucleon moves almost

with the speed of light, because the time dilation effect slows the internal motions such that the wave function of the nucleon can be described as a simple quantum mechanical ensemble of quasireal partons that do not mix with vacuum fluctuations (except for the slowest gluons and sea quarks).

It is convenient to choose the *nucleon-nucleon center-of-mass frame* (c.m.$_{NN}$) in which each nucleon has the same value of longitudinal momentum P (see Fig. 1),

$$P_z^{(p)} = +P \ , \qquad P_z^{(A)} = -AP \ ,$$

$$\mathbf{P}_\perp^{(p)} = \mathbf{P}_\perp^{(A)} = \mathbf{0} \ , \tag{1}$$

so that

$$\sqrt{s} = \sqrt{4AP^2 + M_N^2(1 + A^2)} \tag{2}$$

and

$$\sqrt{s_{NN}} = 2P \ , \tag{3}$$

where A is the nuclear mass number, M_N the nucleon mass, and $P/M_N \gg 1$ is assumed, a requirement which is certainly satisfied at the colliding beam accelerators RHIC and LHC. For example, at RHIC, the maximum P is 250 GeV for $p+p$, 125 GeV for $p+{}^{16}$O, and 100 GeV for $p + {}^{197}$Au [34]. At LHC one has generally a factor of 30 larger energy available [35].

The choice of the c.m.$_{NN}$ frame may appear uncommon for proton-nucleus collisions, since up to now pA experiments are set up as a proton beam incident on a target nucleus at rest. However, at the collider facilities RHIC and LHC the situation is quite different. Both proton and nucleus beams are accelerated and because the beams are bunched, the two opposite beams must have the same Lorentz factor in order to have a stationary beam crossing point. Therefore the center-of-mass energy per nucleon pair $\sqrt{s_{NN}}$ (3), or equivalently P, is the actual measure of the beam energy. Since $\sqrt{s_{NN}}$ is set by the heavy ion, it is the same in pA and in AA col-

FIG. 1. Illustration of the "Lorentz distributed contraction" of proton and nucleus in the c.m.$_{NN}$ frame. The incident proton sees the nucleus as several layers of highly Lorentz contracted nucleons that are surrounded by a cloud of virtual gluons and sea quarks.

lisions. In view of this, the c.m.$_{NN}$ frame is the natural reference frame for these collider experiments. Although I sometimes use the notions "projectile proton" and "target nucleus," I will generally refer to the c.m.$_{NN}$ rather than to the *Laboratory* frame (*Lab*), in which the nucleus is initially at rest, or the *overall center-of-mass frame* (c.m.), except when stated otherwise. Clearly the freedom of choosing a convenient reference frame has only an operational meaning if all observable quantities are independent of the particular choice when properly transformed between different frames. In the PCM this is theoretically guaranteed by the Lorentz invariant form of the transport equation that governs the evolution of the parton phase-space distributions. In the actual simulations however this is a nontrivial issue as has been discussed in Ref. [36].

It is helpful to expose the relation of the c.m.$_{NN}$ with the *Lab* and c.m. frames. Table I summarizes the kinematic connection between the different frames for the various nuclei $A = 1\ldots238$ and the two beam energies $P = 100$ (3000) GeV, corresponding approximately to the maximum achievable energies at RHIC, respectively, LHC. Note that these beam momenta P transform to about $P_{Lab}^{(p)} = 21$ (19 000) TeV incident proton momentum ion the *Lab* frame. For comparison, at the currently highest energy pA experiments performed at the FNAL accelerator, the incident proton has at most $P_{Lab}^{(p)} = 800$ GeV momentum in the laboratory, corresponding to $P \simeq 20$ GeV for $p+{}^{208}$ Pb, and it is questionable if a description on the parton level suffices to account for the gross features of the reactions (see, however, Ref. [14] for attempts to extrapolate down to even ISR energies). In fact, it is expected that $P \gtrsim 100$ GeV roughly marks the energy region where perturbative QCD processes are frequent enough to dominate the dynamics over the underlying soft physics, so that a description based on the parton picture should be reliable.

I would like to briefly recall some important dynamical aspects of pA collisions when described within the parton picture in the c.m.$_{NN}$ frame [18]. In the c.m.$_{NN}$ frame the incident proton sees the nucleus as several layers of highly Lorentz contracted nucleons (Fig. 1) that are surrounded by a cloud of virtual gluons and sea quarks. This "Lorentz distributed contraction" [16,17] was originally pointed out by Bjorken [28] as an important property of partons in high-energy nuclear collisions. When a nucleus together with its nucleons is accelerated, the positions of the nucleons and their valence quarks are boosted from the rest frame of their parent nucleus to the fast moving frame, with the consequence that the valence quarks will be localized in a longitudinally Lorentz contracted region $(\Delta z)_v = 2R_N M_N/P = 2R_N/\gamma$ (R_N and M_N are the nucleon radius and mass, respectively, and γ denotes the Lorentz factor). The gluons and sea quarks on the other hand are smeared out in the z direction by an amount $(\Delta z)_{g,s} = 1/p_z = 1/xP < 2R_N$ around the valence quarks [4,18], where x is the fraction of the parent nucleon's longitudinal momentum carried by the parton. The higher the boost, or P, the smaller the typical x values of gluons and sea quarks in the nucleon structure functions, so that these virtual quanta are more and more
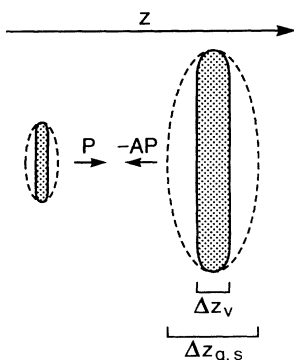
TABLE I. Relation between the *nucleon-nucleon center-of-mass* frame (c.m.$_{NN}$), the *Laboratory* frame (*Lab*) and the *overall center-of-mass* frame (c.m.) in pA collisions for the two values of $P = 100$ GeV and $P = 3000$ GeV and the various nuclear targets considered in this paper.

$$P = P^{(p)}_{\text{c.m.}_{NN}} = -P^{(A)}_{\text{c.m.}_{NN}}/A = 100 \text{ GeV} \qquad (\gamma^{(p)} = \gamma^{(A)} = 106 , \quad y^{(p)} = -y^{(A)} = 5.3)$$

A	$\sqrt{s}$ (GeV)	$P^{(p)}_{Lab}$ (GeV)	$P^{(p)}_{\text{c.m.}}$ (GeV)	$-P^{(A)}_{\text{c.m.}}/A$ (GeV)	$\gamma_{\text{c.m.}}$
1	200	2.1×10^4	100	100	106
8	566	2.1×10^4	283	35	38
16	800	2.1×10^4	400	25	27
32	1132	2.1×10^4	565	18	19
56	1498	2.1×10^4	748	13	14
108	2081	2.1×10^4	1038	10	10
197	2813	2.1×10^4	1401	7	8
238	3094	2.1×10^4	1539	6	7

$$P = P^{(p)}_{\text{c.m.}_{NN}} = -P^{(A)}_{\text{c.m.}_{NN}}/A = 3000 \text{ GeV} \qquad (\gamma^{(p)} = \gamma^{(A)} = 3191 , \quad y^{(p)} = -y^{(A)} = 8.7)$$

A	$\sqrt{s}$ (GeV)	$P^{(p)}_{Lab}$ (GeV)	$P^{(p)}_{\text{c.m.}}$ (GeV)	$-P^{(A)}_{\text{c.m.}}/A$ (GeV)	$\gamma_{\text{c.m.}}$
1	6000	1.9×10^7	3000	3000	3191
8	16971	1.9×10^7	8485	1061	1128
16	24000	1.9×10^7	12000	750	798
32	33941	1.9×10^7	16971	530	564
56	44900	1.9×10^7	22450	401	426
108	62354	1.9×10^7	31177	289	307
197	84214	1.9×10^7	42107	214	227
238	92564	1.9×10^7	46282	194	207

smeared out around the increasingly contracted nucleons. As a consequence of this property the thickness of a fast moving nucleus (in longitudinal direction) is never less than $\Delta z \simeq 1$ fm. An equivalent picture also applies of course to a single nucleon. The implication of the Lorentz distributed contraction is that for boosts greater than a critical Lorentz factor $\gamma_c \sim 2.4 A^{1/3}$ (which follows the knowledge of the nuclear size), the partons roughly fall into two distinct rapidity regions [28]: The hard partons with rapidity $y \gtrsim y_0 = y_{\max} - \ln \gamma_c$ belong to the "naive" nucleus, where $y_{\max} \simeq \ln(2P/M_N)$. These partons are essentially the valence quarks with longitudinal extent Δz_v and consequently their number is $N_v \propto A$. The softer partons with $y \lesssim y_0$ belong to the layer of virtual gluons and sea quarks that couple to the valence quarks and that coat the surface of the Lorentz contracted nucleus, smeared out over $\Delta z_{g,s}$. Therefore, $N_{g,s} \propto A^{2/3}$, rather than strictly proportional to A.

The correlation between longitudinal space-time and rapidity, already present in the initial state before the collision, is a very important property that continues to govern the reaction dynamics up to the formation of final hadrons, and therefore must be reflected in the inclusive particle spectra [5]. This issue will be discussed in Sec. IV A.

B. The parton cascade model

Let me briefly review the essential aspects of the PCM. For a detailed description of this model and its applica-

tions I refer to Refs. [5,36], respectively Ref. [6]. In order to investigate the space-time evolution of the parton distributions, one needs to extend the usual momentum space description to full six dimensional phase-space and time. Efforts to formulate a rigorous quantum kinetic theory for QCD have been made [37], but due to the non-Abelian character of the theory, a number of unresolved conceptual and technical problems prevent yet a practical application to concrete problems. An alternative approach is realized in the PCM as a semiclassical kinetic approach based on perturbative QCD and the improved parton model which evolves the partons' phase-space distributions in real time and space. The microscopic dynamics of the dissipative QCD interactions among quarks and gluons during the early stage of a nuclear collision is simulated as the evolution of multiple internetted parton cascades. The corresponding space-time evolution of the partons' phase-space densities $F_a(p,r)$ for the partons of species a (quarks q_f, antiquarks $\bar{q}_f$, of flavor f, or gluons g), is obtained by solving a Boltzmann type, relativistic transport equation using Monte Carlo methods. This transport equation can be expressed in Lorentz invariant form as $[p^\mu \equiv p = (E, \mathbf{p}), r^\mu \equiv r = (t, \mathbf{r}), \partial_\mu \equiv \partial/\partial r^\mu]$,

$$p^\mu \partial_\mu F_a(p,r) = \sum_{\text{processes } k} I_a^{(k)}(p,r) , \qquad (4)$$

with a free-streaming term on the left-hand side and a collision term on the right-hand side,

$$\sum_{\text{processes } k} I_a^{(k)}(p,r) = \sum_{b,c,d} \left\{ j_{cd \to ab}^{\text{gain}}(p,r) - j_{ab \to cd}^{\text{loss}}(p,r) \right\}$$

$$+ \sum_{b,c} \left\{ k_{c \to ab}^{\text{gain}}(p,r) - k_{a \to bc}^{\text{loss}}(p,r) \right\} + \sum_{b,c} \left\{ l_{bc \to a}^{\text{gain}}(p,r) - l_{ab \to c}^{\text{loss}}(p,r) \right\} . \tag{5}$$

This collision term balances the various interaction processes k by which a parton of type a with four-momentum p and position r may be gained or lost in a phase-space volume $d^3p\,d^3r$ around $\mathbf{p}$ and $\mathbf{r}$ at time t. The collision integrals j, k, and l are implicitly dependent on the phase-space densities F_a and involve "effective matrix elements" for the various $2 \to 2$, $1 \to 2$, and $2 \to 1$ processes that are taken into account in terms of the corresponding Born amplitudes plus Sudakov form factors for the in- and outgoing partons. The explicit form of the collision integrals j, k, l, is given in Ref. [36], where also the assumptions underlying the transport equation and its shortcomings are discussed. The time evolution of the partons' phase-space distributions $F_a(p,r)$ according to the kinetic equation (4) can be simulated as a succession of multiple parton-parton collisions together with associated radiative emissions (branchings) and absorption (fusion) processes, once the incoming nuclear parton clouds begin to overlap and interact.

I would like to stress that a number of important effects that characterize the space-time evolution of a many-parton system in nuclear collisions are accounted for [5,36]: nuclear shadowing effects affecting the parton substructure of nuclei, the individual time scale of each parton-parton collision and the formation time of parton radiation, the effective suppression of radiative emissions from virtual partons due to an enhanced absorption probability of others in regions of dense phase-space occupation, and the effects of soft gluon interference in low energetic gluon emissions.

Another important point to be mentioned is the well known fundamental problem: both the perturbative QCD cross sections and the amplitudes for parton emissions are plagued by infrared divergences, which must be regularized. In the PCM this is done by requiring a minimum momentum transfer $p_{\perp 0}$ for semihard and hard parton collisions and a minimum virtuality μ_0 for parton emissions. These parameters of the model are fixed by experimental data for the pp $(p\bar{p})$ cross sections [38] and e^+e^--annihilation [5], respectively. For instance, the parton-parton cross section for the elementary $2 \to 2$ process $a+b \to c+d$ is divided into a (semi)hard contribution for scatterings above $p_{\perp 0}$ that is described by perturbative QCD, and a soft contribution for scatterings below $p_{\perp 0}$ that models the underlying nonperturbative physics. The parameter $p_{\perp 0}$ is a function of beam energy s and is parametrized as $p_{\perp 0}(s) = a(s/s_0)^b$ with $s_0 = 1$ GeV^2 and the parameters $a = 0.35$ GeV and $b = 0.14$ determined such that the parton cross section at a given s yields the correct inelastic nucleon nucleon cross section [38]. The complementation of both contributions renders the parton cross section $d\hat{\sigma}/dp_{\perp}^2$ is well defined for $all\ p_{\perp}$.

At the end of the perturbative QCD phase the hadronization is modeled as a recombination of the fi-

nal state partons to form color singlet clusters, followed by the fragmentation of these clusters into observable hadronic states. It was demonstrated in Ref. [5] that the parton cascade model combined with this cluster hadronization scheme sets a consistent framework to simulate and study the time evolution of hadron-hadron and nucleus-nucleus collisions in complete phase-space, from the first instant of collision to the final particle yield.

III. PROPERTIES OF PARTON CASCADES IN DENSE NUCLEAR MATTER

A. Unitarity and the saturation of the parton densities

In the parton picture for high-energy nuclear reactions a pA collision may be viewed as a diffusion of the partons of the projectile proton, traversing the nucleus and interacting frequently with partons belonging to different target nucleons [14,39]. I will distinguish between *primary* and *secondary* particles: The particles that are present already in the initial state as part of the proton and nucleus wave function are termed "primary," whereas all particles that have interacted at least once, plus those that are newly formed during the reaction, are labeled "secondary." Thus, a primary parton that belongs to the initial proton is a spacelike virtual particle, because it is bound and confined inside the proton. This parton can become a secondary one by means of a collision with one of the nuclear partons, because the interaction sets it free and provides it with enough energy to propagate as a real, timelike excitation. Such a parton probes the nuclear environment as it evolves further by initiating a cascade of secondary partons due to three different types of interactions with the nuclear medium:

(i) The incident parton can collide with partons of the nucleus and scatter those out of the coherent bound state of the nucleon to which they belong; (ii) it can radiate bremsstrahlung gluons; (iii) it may absorb (fuse with) partons of the nucleus.

In addition, of course, there will be similar interactions among partons belonging to different cascades. The so produced secondary partons will subsequently undergo the same type of interactions, until all of the primary energy has been dissipated. The processes (i) and (ii) both lead to a rapid entropy production by multiplication of partons that increases the local density and consequently the probability for rescatterings [12]. This parton multiplication results in a dense phase-space population at small energy fractions $x \ll 1$, corresponding to partons with comparably small energies of $\sim 1 - 3$ GeV, so that at some point the probability for a parton to interact

with this dense parton matter tends to become larger than unity, which means that the unitarity principle is violated. This occurs when the partons are so densely packed that they spatially overlap in transverse direction [17,40] and the nucleus appears to be completely black. However, following Levin and Ryskin [14], this unpleasant feature can be resolved by consistently taking into account the fusion processes (iii): these must become increasingly important as the phase-space density grows, until a detailed balance between branching and fusion processes yields a local saturation of the parton density and stops a further increase. Indeed, such a saturation behavior has been experimentally observed in pp ($p\bar{p}$) collisions by studying the inelastic scattering amplitude as a function of energy and of impact parameter [41].

At this point I would like to comment on the conventional procedure of unitarization that is commonly used for the cross section in hadronic collisions [42,43]. In this approach, the eikonal formalism for the impact parameter representation of hadron collisions relates the energy dependent pp ($p\bar{p}$) total and inelastic cross section with the microscopic parton-parton cross section. Also in the PCM this procedure is employed [38] in order to determine the magnitude of the parton cross section and to define the boundary between semihard and hard perturbative processes and underlying soft nonperturbative processes, as mentioned at the end of Sec. II. For hadron-hadron collisions this is sufficient, since at present, collider energies in hadronic collisions fusion and absorption processes are irrelevant. However, when proceeding to pA or AA collisions, those additional interactions will play an important role for the particle production, if the density of partons in phase space becomes very large. It is one of the main features of the PCM that it indeed predicts such a density increase as compared to pp col-

lisions. In collisions involving heavy nuclei, one cannot simply treat each individual parton scattering as an interaction equivalent to a single parton scattering in pp. This can lead to a dramatic overestimate of the particle multiplicities, because of the immense gluon multiplication at small rapidity triggered by multiple scatterings. To ensure that the additional effects of partons cascading in a dense nuclear environment do not violate the unitarity principle, a supplemental criterium for unitarization must be set up.

To be specific: unitarity conservation states that the sum of probabilities of all elastic plus inelastic reaction channels must not exceed unity. This requirement can be ensured by implementing the Gribov-Levin-Ryskin unitarity condition [13,14]. In order to implement this condition in the framework of the PCM, let me introduce the total interaction probability W_a of a given parton of species a to collide with another parton around and $\mathbf{r}$ and $\mathbf{r} + \Delta\mathbf{r}$ at time t within some time interval t and $t + \Delta t$, where the time is measured in the c.m.$_{NN}$ reference frame. The interval Δt must be smaller than the typical mean free path in order to resolve the frequency of successive scatterings (in the simulations I choose $\Delta t = 10^{-2}$ fm). The parton-parton collision can either be an elastic scattering with two outgoing partons, or it may be an inelastic collision in which case there will be $n > 2$ partons resulting from the interaction (see Fig. 2). Thus, the total probability W_a is a sum of contributions from scatterings of a parton a with all kinds of partons b, that become scattering candidates within Δt. It is integrated over the volume which the parton a traverses during the time span Δt, as well as integrated over the momentum and weighted by the phase-space distribution of those partons b present in this volume (see Fig. 3):

$$W_a(p_a, \mathbf{r}, \Delta t) := \Delta t \sum_b \int_z^{z+\Delta z} dz \int_0^{R_A} d^2 r_\perp \; w_{ab}(p_a, \mathbf{r}, \Delta t) \; , \tag{6}$$
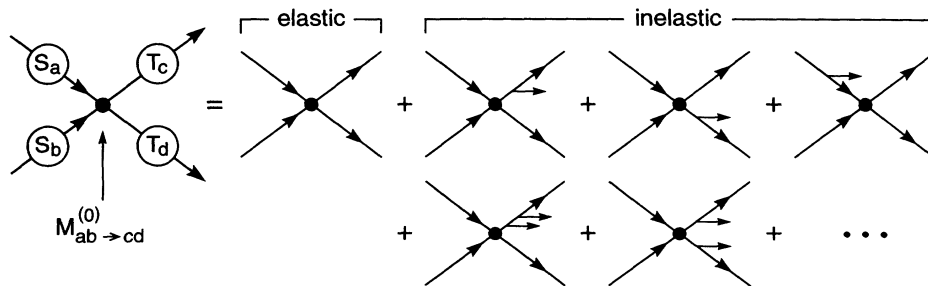
FIG. 2. Graphical representation of the "effective" matrix-elements (8), in which each of the particles coming in and going out of an elementary vertex, is "dressed" with a specific form factor (spacelike S or timelike T) that takes into account the higher order corrections to the elementary Born terms. The lowest order Born amplitude $M^{(0)}_{ab \to cd}$ corresponds to elastic $2 \to 2$ scattering, and the form factors inclusively sum up all inelastic $2 \to n$ contributions associated with emission of n additional particles.

with

$$w_{ab}(p_a, \mathbf{r}, \Delta t) = \frac{1}{2E_a} \frac{S_{ab}}{\gamma_a \gamma_b} \int \frac{d^3 p_b}{(2\pi)^3 2E_b} \gamma_b F_b(p_b, \mathbf{r}, t)$$

$$\times \int \frac{d^3 p_c}{(2\pi)^3 E_c} \int \frac{d^3 p_d}{(2\pi)^3 E_d} \left[\sum |\mathcal{M}_{ab \to cd}|^2_{\text{eff}}(p_a, p_b, q^2) \right] \delta^4(p_a + p_b - p_c - p_d) \ . \tag{7}$$

The structure of the collision probability w_{ab} is as follows. The $(2E_a)^{-1}$ is the flux factor, $S_{ab} = (1 + \delta_{ab})^{-1}$ is due to the identical particle effect, and the factor $(\gamma_a \gamma_b)^{-1}$ comes from averaging over the degeneracies of the colliding partons in spin and color space ($\gamma_g = 2 \times 8$, $\gamma_q = \gamma_{\bar q} = 2 \times 3$). The phase-space distribution F_b is multiplied by the degeneracy factor γ_b, because one must sum over spin and color of the partons b. Pauli-blocking and Bose-enhancement factors for the outgoing partons c and d are omitted here. Finally, the "effective" squared matrix elements $\sum |\mathcal{M}|^2_{\text{eff}}$ depend on the invariant mass $\hat{s} = (p_a + p_b)^2$ as well as on the squared momentum transfer $q^2 = (p_a - p_c)^2 = (p_b - p_d)^2$, and are expressed in terms of the lowest order matrix elements, $\sum |M^{(o)}|^2$, summed over spin and color, and are multiplied by S (spacelike) and T (timelike) form factors for the partons a, b coming in, respectively, partons c, d going out of, the vertex,

$$\sum |M_{ab \to cd}|^2_{\text{eff}} = S_a(p_a; q^2) \, S_b(p_b; q^2)$$

$$\times \left[\sum |M^{(o)}_{ab \to cd}|^2(p_a, p_b, q^2) \right]$$

$$\times T_c(q^2) \, T_d(q^2) \ . \tag{8}$$

The lowest order invariant squared matrix elements $\sum |M^{(o)}|^2$ are the well known expressions for the elementary parton-parton scatterings [44], and the explicit form of the Sudakov form factors S and T are given in Refs. [5,36]. The form factors represent the nonbranching probability of the partons coming in (emerging from) the scattering vertex and take into account the higher order corrections in the leading logarithmic approximation to the lowest order Born terms. For purely elastic scatterings $S = T = 1$, so that the effective squared matrix
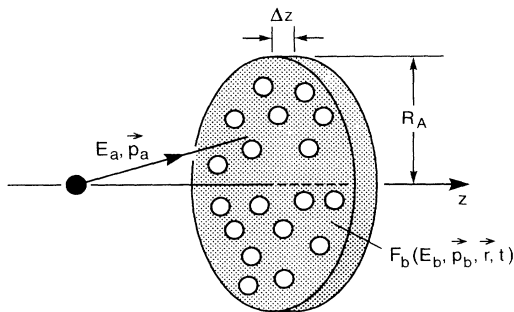

FIG. 3. A parton a under consideration can interact during a time span Δt with all kinds of partons b, that are contained in the volume $\Delta z \pi R^2_A$ which the parton a traverses within Δt. The density of scatterers F_b determines the magnitude of the interaction probability W_a.

element (8) reduces to the elementary Born amplitude squared. This is graphically illustrated in Fig. 2.

To elucidate the physical meaning of W_a, consider a simplified case where the higher order corrections are omitted and only elastic scattering processes are accounted for. Furthermore, suppose one can approximate the spatial part of the phase-space density F_b by the average number of partons contained in $\Delta z \pi R^2_A$,

$$n_b(y, p^2_\perp, t) = \frac{N_b(y, p^2_\perp, t)}{\Delta z \pi R^2_A}$$

$$\equiv \frac{1}{\Delta z \pi R^2_A}$$

$$\times \int_z^{z + \Delta z} dz \int_0^{R_A} d^2 r_\perp \, \gamma_b F_b(p_b, \mathbf{r}, t) \tag{9}$$

that can be resolved by the incident parton a at the scale $p^2_\perp$ and that are contained in a disc of transverse radius R_A and length Δz. [Here $p^2_\perp$ denotes the squared transverse component of $q \equiv (\omega, p_z, p_\perp)$.] The situation is illustrated in Fig. 3. In this approximation one gets a rough estimate for W_a within the interval $[z, z + \Delta z]$,

$$W_a(y, \Delta z, \Delta t) \approx \Delta t \frac{1}{\Delta z \, \pi R^2_A}$$

$$\times \int_{q^2_{\perp 0}}^\infty dp^2_\perp \, N_b(y, p^2_\perp) \left(\frac{d\hat{\sigma}_{ab}(p^2_\perp)}{dp^2_\perp} \right) \ , \tag{10}$$

where

$$\frac{d\hat{\sigma}_{ab}(p^2_\perp)}{dp^2_\perp} = \frac{1}{16\pi \hat{s}^2} \sum |M^{(o)}_{ab \to cd}|^2(\hat{s}, p^2_\perp) \, \theta(\hat{s} - 4p^2_\perp) \ . \tag{11}$$

Approximating the parton-parton cross section by its small-angle scattering part, i.e., keeping only the $1/p^2_\perp$ terms which give the dominant contribution at small rapidities and small $p^2_\perp$ (the semihard region), one finds

$$W_a(y, \Delta z, \Delta t) \approx \frac{\Delta t}{\Delta z} \frac{\bar{N}_b(y, p^2_{\perp 0}), t}{\pi R^2_A} \frac{\pi \alpha^2_s}{p^2_{\perp 0}} c_{ab} \ , \tag{12}$$

with $\bar{N}_b(y, p^2_\perp, t) = \int^{p^2_\perp} dp^{2\prime}_\perp N(y, p^{2\prime}_\perp, t)$. The momentum scale $p^2_{\perp 0} > 1$ GeV is a parameter that cuts off the infrared divergence in the cross section for vanishing momentum transfer and c_{ab} is a constant, e.g., for gg scattering, $c_{gg} = 9/2$. Physically this divergence must be canceled: In the beginning of the reaction, the inci-

dent proton sees the nucleus as an ensemble of nucleons, so that the divergence must be canceled at distances of a nucleon radius ($p_{\perp 0}^2 \simeq 1/R_N^2$), because only a parton with Compton wavelength $\lambda \simeq 1/p_{\perp}^2$ that is smaller than R_N can resolve the substructure of the nucleons in the nucleus and can interact incoherently with the nuclear partons. At later times, as the coherence of the struck nucleons in the target is progressively destroyed and local deconfinement of the nuclear partons occurs, the divergence must be cured at distances of the order of the Debye screening length [45,46] that naturally cuts off scattering with large impact parameters (as will be discussed in Sec. III C).

In the simplified form (12), the interaction probability W_a is essentially the fraction of transverse area occupied by the partons in a layer Δz per one unit of rapidity. To give an example, let me restrict to gluon-gluon scattering, since the gluonic processes give the dominant contribution [12,24]. The very first collisions that occur are primary scatterings between a gluon g of the projectile proton with a gluon g' of the nucleus, so that for these processes the number of gluons $\bar{N}_{g'}$ seen by the projectile gluon g can be estimated from the nuclear structure functions as [18,40] $\bar{N}_g(y, p_{\perp}^2, t_0) \approx A\, x\, g(x, p_{\perp}^2)$, where $y = \ln x$, A is the mass number of the nucleus, and $g(x, p_{\perp}^2)$ is the gluon number density in a nucleon. Thus,

$$W_g(y = \ln x, \Delta z, \Delta t) \approx \frac{\Delta t}{\Delta z}\, \frac{9}{2}\, \frac{\alpha_s^2(p_{\perp 0}^2)}{R_A^2\, p_{\perp 0}^2}\, A\, x g(x, p_{\perp 0}^2)\ . \tag{13}$$

To obtain a crude estimate, consider a uranium nucleus, $A = 238$, with $R_A = 7.3$ fm at RHIC energy ($P = 100$ GeV). A reasonable estimate for the gluon number density in the semihard region ($p_{\perp} \simeq 1 - 5$ GeV) is $xg \approx 3$, almost independent of x. Taking $\Delta z = \Delta t = 10^{-2}$ fm [47] and a value of $p_{\perp 0}^2 = 1.6$ GeV (as in the actual PCM calculations $P = 100$ GeV) implying $\alpha_s \simeq 0.3$, then one gets $W_g \simeq 0.1$, which is far below the unitarity limit even for the heaviest nucleus. However, it is already found [12,24] that during the very early stage of the nuclear collision (within the first couple of fm), the exponential multiplication [39] of secondary gluons produced in frequent scatterings and gluon bremsstrahlung rapidly increases the number density at small rapidities easily by an order of magnitude. Therefore with progressing time W_g will approach unity, or increase even beyond, in which case one is in trouble because the unitarity principle is violated.

The unpleasant feature of possible unitarity violation can be circumvented by the requirement

$$W_a(y, z, \Delta t) \overset{!}{\leq} 1\ . \tag{14}$$

The physical meaning of this constraint is very simple. Since W_a is proportional to the rapidity density of scatterers n_b, the relation $W_a \ll 1$ will be satisfied as long as n_b is sufficiently dilute. On the other hand, when W_a approaches 1, the probability for the parton a to interact becomes unity, because the density n_b reaches its max-

imum value $n_b^{\max}$ and the parton a sees a black wall of matter in front of it. For even larger densities $n_b > n_b^{\max}$, unitarity conservation is violated: the matter cannot be blacker than black, that is, the interaction probability cannot exceed unity. However, as mentioned before, at large densities n_b the partons begin to spatially overlap in the transverse plane. This means that absorption or fusion processes become essential. Thus, W_a gives the time-dependent probability for the fusion of a given parton a with some other parton b, depending on the local density n_b and the scale of interaction, $p_{\perp}^2$.

The practical implementation of this concept in the PCM is done in the following manner. The time evolution of the parton cascade development is traced in discrete time steps $\Delta t = 0.01$ fm and after each time step a profile of the phase-space densities F_b is calculated by dividing phase-space in cells and estimating the local density of quarks and of gluons in each cell [6]. Within a given time step Δt, for each parton a that is a potential candidate for a collision with some other parton b, the total lowest order $2 \to 2$ parton-parton cross section plus higher order multiple emission probabilities are evaluated, as described in Ref. [5]. Then W_a is calculated according to the full expression (6) and with probability W_a the parton a will undergo a $2 \to 1$ fusion with the other parton b, and with probability $1 - W_a$ it will be an elastic ($2 \to 2$) or inelastic ($2 \to n$) scattering with $n > 2$.

In Fig. 4 the time evolution of the probability W_g for gluons at small rapidities $|y| \leq 1.5$, obtained from the PCM simulations of pA collisions with $P = 100$ GeV and $P = 3000$ GeV, where P is defined in Eq. (1). The quarks and antiquarks play a minor role here, so that W_g can be identified with the total $W = \sum_a W_a$. Common to both beam energies is that for light nuclei $A \lesssim 30$ the fusion probability is only $\simeq 0.2$–0.3, but it already reaches more than 70% for nuclei around $A = 100$, and 90%, respectively 100% for ^{238}U at $P = 100$ (3000) GeV. It is also interesting that the time it takes to increase W_g from 0.1 to 0.9 of its final value is typically a factor of 2 smaller at $P = 3000$ GeV than at $P = 100$ GeV. Furthermore, at fixed P this time scale decreases significantly when pro-
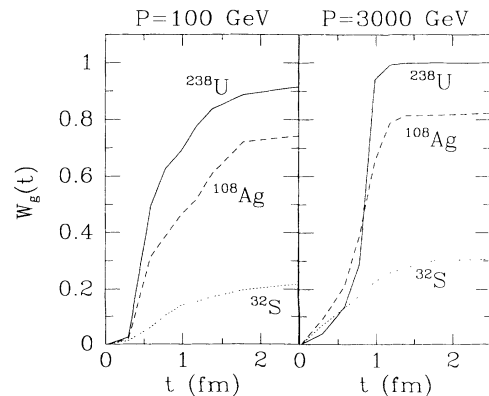

FIG. 4. Increase of the interaction probability W_g for gluons to fuse at small rapidities $|y| \leq 1.5$, obtained from pA simulations at $P = 100$ GeV and $P = 3000$ GeV on the basis of Eq. (6). The time t is measured in the c.m.$_{NN}$ frame.

ceeding from ^{32}S to ^{238}U nuclei. Note that the saturating behavior that is evident even for, e.g., ^{32}S although W_g is far from unity, results from the fact that the duration of the reaction is the smaller the lighter the nucleus is, so that the partons naturally cease to interact (except for some small amounts of residual interactions) when the system flows apart before it finally hadronizes.

B. Soft interactions versus perturbative parton fusion

It is a well known fundamental problem that the perturbative QCD cross sections are plagued by infrared divergences, which have to be regularized. In the PCM this is done by introducing a scale $p_{\perp 0}^2$ that separates the perturbative regime from the nonperturbative domain. Accordingly the total invariant cross section for the scattering of two partons a and b is represented as [5]

$$\hat{\sigma}_{ab}(\hat{s}, p_{\perp 0}^2) = \sum_{c,d} \left\{ \int_0^{p_{\perp 0}^2} dp_\perp^2 \left(\frac{d\hat{\sigma}_{ab \to cd}^{\text{soft}}}{dp_\perp^2} \right) \right.$$
$$\left. + \int_{p_{\perp 0}^2}^\infty dp_\perp^2 \left(\frac{d\hat{\sigma}_{ab \to cd}^{\text{hard}}}{dp_\perp^2} \right) \right\} \quad . \quad (15)$$

Here $p_\perp^2$ is the relative transverse momentum produced that defines the interaction scale, $\hat{s}$, $\hat{t}$, and $\hat{u}$ are the usual Mandelstam variables and the sum over c, d corresponds to summing over all possible reaction channels (i.e., final states). The differential cross sections $d\hat{\sigma}_{ab \to cd}^{\text{soft}}/dp_\perp^2$ are given in Ref. [36] and for $d\hat{\sigma}_{ab \to cd}^{\text{hard}}/dp_\perp^2$ the standard expressions in the literature [44] are employed. To render $\hat{\sigma}_{ab}(\hat{s})$ finite, the $p_\perp$ range is divided by an invariant scale $p_{\perp 0}$ such that for $p_\perp \geq p_{\perp 0}$ the perturbative QCD cross section $\hat{\sigma}_{ab \to cd}^{\text{hard}}$ is applied, whereas for $p_\perp < p_{\perp 0}$ a phenomenological, exponentially damped (as $p_\perp \to 0$) soft cross section $\hat{\sigma}_{ab \to cd}^{\text{soft}}$ is employed [5]. The scale $p_{\perp 0}$ is a parameter of the model that determines how much of the cross section is assigned to truly perturbative QCD processes. Its value generally depends on the beam energy $\sqrt{s}$ of the nuclear collision system $A + B$ and is taken from the following parametrization [38], obtained from an analysis of the measured pp ($p\bar{p}$) cross sections up to TeV collider energies,

$$p_{\perp 0}^2 = a \left(\frac{s_{NN}}{s_0} \right)^{2b} , \quad (16)$$

where $a = 0.35$ GeV/c, $b = 0.14$, $s_0 = 1$ GeV^2, and $\sqrt{s_{NN}} = 2\sqrt{s}/(A + B)$ is the center-of-mass energy per nucleon pair.

Now I will argue that the unsatisfactory model phenomenology of nonperturbative soft interactions can be traded against a parameter-free perturbative description of parton-parton fusion. In the previous section I explained that the unitarity constraint limits the growth of the number of partons and ensures that the total inelastic cross section does not violate unitarity. As a consequence of increasingly prominent parton fusion processes at high

densities, involving mostly soft partons with comparably small transverse momenta (of a few GeV), the parton densities must saturate locally at some value $p_{\perp 0}$ [cf. Eq. (9)]. This issue was investigated in detail by Levin and Ryskin [13]. The authors presumed that for pp ($p\bar{p}$) collisions the characteristic value $p_{\perp 0}$ is the typical transverse momentum of partons at the point when the fusion probability W, Eq. (6), approaches unity. They found a beam energy dependent behavior

$$\tilde{p}_{\perp 0}^2 = Q_0^2 + \Lambda^2 \exp(2.52\sqrt{\ln s}) \quad (17)$$

with the parameters $Q_0 = 1.4$ GeV and $\Lambda = 52$ MeV determined from fitting the inclusive hadron spectra at the CERN $p\bar{p}$ collider. For example, the values of $\tilde{p}_{\perp 0}$ for pp collisions at 200, 1800, and 6300 GeV are $\tilde{p}_{\perp 0} = 2.0$, 3.3, 4.7 GeV, respectively. This is rather similar to the parametrization (16) of the parameter $p_{\perp 0}$ in the PCM, which gives the corresponding values $p_{\perp 0} = 1.6$, 2.9, 4.1 GeV, respectively. Therefore it seems plausible to identify $p_{\perp 0}$ with the lower bound of $\tilde{p}_{\perp 0}$ and associate with it the characteristic momentum scale below which the parton fusion processes occur with probability $W \simeq 1$ and guarantee a constant behavior of the parton densities for $p_\perp < p_{\perp 0}$.

From this point of view it is suggestive to replace in the PCM the model-dependent soft scattering processes by parton-parton fusion processes within perturbative QCD. These $2 \to 1$ recombinations are treated on the same footing as the perturbative $2 \to 2$ parton-parton scatterings, as explained in Ref. [36]. Thus, rather than trying to mimic the underlying soft physics phenomenologically, all parton interactions are treated now on an equal basis, within perturbative QCD and the statistical parton picture. Note that only fusion processes among timelike partons are taken into account, recombinations between partons in the nuclear structure functions have been estimated to be negligible at the energies considered here [40]. As explained in the preceding section these perturbative fusion processes can also occur in the regime $p_\perp > p_{\perp 0}$ with the probability W, Eq. (6), that varies between 0 in vacuum and 1 in ultradense matter. However for $p_\perp < p_{\perp 0}$, the fusion probability W is assumed to always equal 1, so that the only way two partons can interact is by fusion. This naturally leads to a saturation of the parton density around the particular value of $p_{\perp 0}$ that corresponds to the beam energy $\sqrt{s}$ according to (16). The infrared divergent behavior of the perturbative parton-parton cross section is then regularized by the parton dynamics itself.

In Fig. 5 the differential parton-parton cross section, summed over all particle species and interaction channels,

$$\frac{d\hat{\sigma}}{dp_\perp^2} = \sum_{ab} \frac{d\hat{\sigma}_{ab}}{dp_\perp^2} , \quad (18)$$

where $\hat{\sigma}_{ab}$ is defined in (15), is shown for $P = 100$ GeV and $P = 3000$ GeV versus the relative transverse momentum $p_\perp$ associated with the interaction in the center-of-mass frame of the parton pair. It is evident that the infrared divergence at $p_\perp = 0$ is damped out and renders the cross section finite for any $p_\perp$. It is peaked around
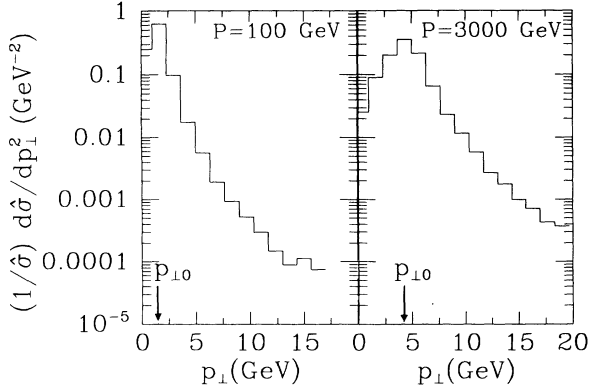
FIG. 5. The differential parton-parton cross section (18), summed over all particle species and interaction channels, for $P = 100$ GeV and $P = 3000$ GeV vs the relative transverse momentum $p_\perp$ associated with the interaction in the center-of-mass frame of the parton pair. The cross section is peaked around the energy dependent $p_{\perp 0}$ value (16) which characterizes the typical momentum transfer at a given beam energy, and is damped at $p_\perp \to 0$, avoiding an infrared divergence.

the energy-dependent $p_{\perp 0}$ value (16) which characterizes the typical momentum transfer at a given beam energy. Of course the scale parameter $p_{\perp 0}$ still enters as the defining lower boundary of the perturbative QCD domain and remains an unsatisfactory arbitrariness. In the following section I will argue that the value of $p_{\perp 0}$ can be estimated self-consistently from the parton evolution itself, provided that the local parton density is large enough to screen the long range color forces which are the origin of the singular behavior of the cross sections.

C. Dynamical screening in parton-parton collisions

To determine whether a given parton a will collide with some other parton b within a time step Δt, for all possible collision partners b the total perturbative cross section in Born approximation,

$$\hat{\sigma}_{ab}(\hat{s}, p_{\perp 0}^2) = \sum_{c,d} \int_{p_{\perp 0}^2}^{\infty} dp_\perp^2 \left(\frac{d\hat{\sigma}_{ab \to cd}^{hard}}{dp_\perp^2} \right) \quad , \quad (19)$$

is calculated by integrating the lowest order differential cross sections [44] over the kinematically allowed range and summing over all final states. This cross section is used to define an effective area of interaction with radius

$$\hat{b}_{ab}^{max}(p_{\perp 0}^2) = \sqrt{\frac{\hat{\sigma}_{ab}(\hat{s}, p_{\perp 0}^2)}{\pi}}, \quad (20)$$

which sets the maximum allowed impact parameter for the parton pair under consideration. Thus, in a given time interval Δt the two partons can only collide if the distance d_{ab} between them satisfies

$$d_{ab} \leq d_{ab}^{min} = \sqrt{(\hat{b}_{ab}^{max})^2 + (\Delta t)^2} \quad . \quad (21)$$

If this is the case, it now has to be checked, (i) whether the partons a and b will pass their point of closest approach, and, (ii) if this distance of closest approach is smaller than $\hat{b}_{ab}^{max}$. In the center-of-mass frame of the partons a and b, their momenta are $\mathbf{p}_{c.m.}$ and $-\mathbf{p}_{c.m.}$, respectively, and the distance $\Delta \mathbf{r} = \mathbf{r}_a - \mathbf{r}_b$ in the lab frame becomes in the center-of-mass frame $\Delta \mathbf{r}_{c.m.} = (\hat{\gamma} - 1)(\Delta \mathbf{r} \cdot \boldsymbol{\beta}/\beta)\boldsymbol{\beta}/\beta + \Delta \mathbf{r}$, where $\hat{\gamma} = (1 - \beta^2)^{-1/2}$ and $\boldsymbol{\beta}$ is the velocity of the center-of-mass of a and b. Thus the two partons will collide within the time interval $\Delta t/2$ and $+\Delta t/2$, if (i)

$$\left| \frac{\Delta \mathbf{r}_{c.m.} \cdot \mathbf{p}_{c.m.}}{p_{c.m.}} \right| < \left(\frac{p_{c.m.}}{E_{1\,c.m.}} + \frac{p_{c.m.}}{E_{2\,c.m.}} \right) \frac{\Delta t}{2} \quad , \quad (22)$$

and if (ii) [48]

$$\hat{b}_{ab} = \sqrt{(\Delta \mathbf{r}_{c.m.})^2 - \left(\frac{\Delta \mathbf{r}_{c.m.} \cdot \mathbf{p}_{c.m.}}{p_{c.m.}} \right)^2} < \hat{b}_{ab}^{max} \quad . \quad (23)$$

Now the crucial point in this approach is that the maximum allowed impact parameter (20) depends sensitively on $p_{\perp 0}$, because the cross section $\hat{\sigma}_{ab}$ rises at small momentum transfers as $1/p_{\perp 0}^2$. Therefore already a small variation of $p_{\perp 0}$ results in a sizable change of the collision probability, since the effective interaction area varies as $\pi(\hat{b}_{ab}^{max})^2 = \hat{\sigma}_{ab}(\hat{s}, p_{\perp 0}^2)$. However, this sensitivity can be overcome, provided the density of scatterers is sufficiently large, by implementing a dynamical screening of the divergent long wavelength contributions to the interaction probability. The previous method in the PCM of selecting for the given parton a a collision partner was to choose the first encountered parton b that satisfies the conditions (22) and (23). That completed the search for parton a, since each parton can only have one collision partner within Δt. Instead of employing this rather arbitrary selection procedure, I now propose the following prescription. All possible collision partners b are considered equal candidates for the actual scattering pair a and b. In case there is more than one collision partner for a, the one with the minimum impact parameter

$$\hat{b}_{ab}^{min} = \min_{b=1,\dots,n} [\,\hat{b}_{ab}\,] \quad (24)$$

is chosen, where n is the number of potential candidates b that satisfy (22) and (23). This is illustrated in Fig. 6. In nuclear collisions, pA or AB, involving at least one heavy nucleus $(A \gg 1)$, the population of partons in the central region becomes very dense [6], so that the probability of finding $n > 1$ collision candidates is almost unity. In particular, if $n \gg 1$, then

$$\frac{\hat{b}_{ab}^{min}}{\hat{b}_{ab}^{max}(p_{\perp 0}^2)} \ll 1 \quad , \quad (25)$$

and a variation of the parameter $p_{\perp 0}$ that leads to a significant change of b_{ab}^{max}, say by a factor of 5, does not affect the choice of the actual collision partner b for the
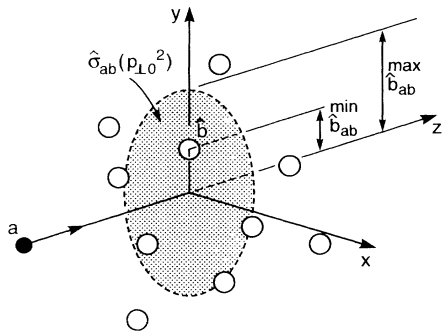
FIG. 6. Illustration of the prescription for choosing for a given parton a the collision partner b. Of all potential scattering candidates b contained within the effective interaction area $\pi(\hat{b}_{ab}^{max})^2$, given by the cross section $\hat{\sigma}_{ab}(p_{\perp 0}^2)$, the one with the minimum impact parameter $\hat{b}_{ab}^{min}$ is selected.

parton a with $\hat{b}_{ab} = \hat{b}_{ab}^{min}$. The parameter $p_{\perp 0}$ loses its sensitive influence and the infrared divergence of the cross section $\hat{\sigma}_{ab}$ is naturally cut off at

$$(p_{\perp 0})_{ab} \equiv \frac{1}{b_{ab}^{min}} > p_{\perp 0} \ . \tag{26}$$

In other words, the long range part of the Coulomb-type color field is screened below $(p_{\perp 0})\text{vert}_{ab}$. Thus, each collision pair has its individual value of $(p_{\perp 0})_{ab}$, depending on the local density of surrounding partons. Consequently, when selecting the scattering angle $\hat{\theta}_{c.m.}$ for a chosen subprocess $ab \to cd$ from the probability distribution

$$\Xi(p_\perp^2) = \frac{1}{\hat{\sigma}_{ab \to cd}} \int_{(p_{\perp 0}^2)_{ab}}^{p_\perp^2} dp_\perp'^2 \left(\frac{d\hat{\sigma}_{ab \to cd}}{dp_\perp'^2}\right) \ , \tag{27}$$

the small-angle scattering is bounded by $\cos\hat{\theta}_{c.m.} > 1 - 2p_{\perp 0}^2/\hat{s}$, which is set by the dynamics of the parton system itself and not by an "external" parameter.

In Fig. 7 the time evolution of the impact parameter distribution of parton-parton collisions $dN^{coll}/d\hat{b}$ is compared for the case of proton-gold collisions at $P = 100$ GeV, respectively $P = 3000$ GeV. The three histograms in each plot refer to the different time spans $0 < t < 0.5$ fm, $0.5 < t < 1.2$ fm, and $1.2 < t < 3$ fm. As before, t refers to the c.m.$_{NN}$ frame, and $t = 0$ is the moment of penetration. Figure 8 on the other hand shows the A dependence of the average impact parameter $\langle\hat{b}\rangle$, obtained from accumulated statistics of all parton-parton scatterings during the first 3 fm in pA collisions at the two considered energies. The most evident features are:

(i) There is a characteristic evolution pattern in both the width and the height of the impact parameter distributions $dN^{coll}/d\hat{b}$, which starts with a flat distribution, that subsequently steepens and contracts in width, and finally flattens out and becomes broader again;

(ii) the values of $\langle\hat{b}\rangle$ change insignificantly for light nuclei $(A \leq 32)$, then significantly decrease roughly as $A^{-1/6}$ as one proceeds to heavier nuclei, and finally seem to saturate for very heavy nuclei.
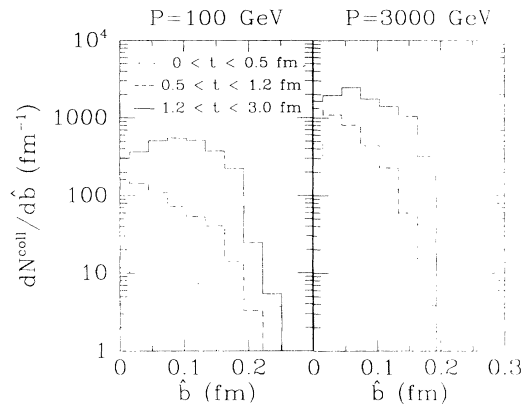

FIG. 7. Time evolution of the impact parameter distribution of parton-parton collisions $dN^{coll}/d\hat{b}$ in $p + ^{197}$Au collisions at $P = 100$ GeV, respectively $P = 3000$ GeV. The three histograms in each plot refer to the different time spans $0 < t < 0.5$ fm, $0.5 < t < 1.2$ fm, and $1.2 < t < 3$ fm, where t refers to the c.m.$_{NN}$ frame and $t = 0$ is the moment of nuclear contact of penetration.

The point (i) can be understood as follows. The rather flat impact parameter distribution during the early stage $0 < t < 0.5$ fm (dotted histograms in Fig. 7) is generated by mostly primary parton-parton scatterings for which the typical impact parameter $\hat{b}$ is of the order of $\hat{b}^{max}(p_\perp^2)$, Eq. (20). At this point the initial nuclear parton density, taken from the nuclear structure functions, is yet too dilute to provide a dynamical screening. The average $\langle\hat{b}\rangle$ that corresponds to these early collisions is about 0.18 fm for $P = 100$ GeV, and 0.12 fm for $P = 3000$ GeV. These values reflect the typical geometric parton-parton cross section. During the second stage $0.5 < t < 1.2$ fm (dashed histograms) the parton density increases significantly due to intense gluon bremsstrahlung initiated by the comparably hard primary scatterings. This not only
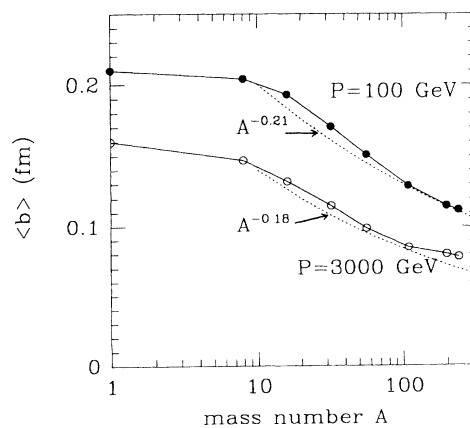

FIG. 8. Dependence of the average impact parameter $\langle\hat{b}\rangle$ on the mass number A in pA collisions up the first 3 fm after the interpenetration of the proton for the two considered beam momenta $P = 100$ GeV and $P = 3000$ GeV.

increases the interaction probability as obvious from the height of the distributions, but also parton scatterings are now clearly affected by the screening mechanism, and the values for $\langle \hat{b} \rangle$ during this stage decrease compared to the first stage to 0.11 (0.08) fm for $P = 100$ (3000) GeV. The third stage $1.2 < t < 3$ fm (full histogram) is dominated by scatterings involving momentum transfers around $p_{\perp 0}$ that are mostly elastic and do not contribute to additional particle creation. In fact, most of the initial energy is dissipated at this stage and the matter becomes more dilute by streaming apart. This is reflected by an increase of $\langle \hat{b} \rangle$ compared to the second stage, namely now $\langle \hat{b} \rangle \simeq 0.13$ (0.10) fm for $P = 100$ (3000) GeV.

The observation (ii) is consistent with what one would expect from the following geometrical consideration. As explained in Sec. II A, due to the Lorentz distributed contraction, the longitudinal size of a fast moving nucleus is always $\simeq 1$ fm. Now the number of nucleons that would fit in a slab of $\Delta z = 1$ fm in longitudinal direction is $2r_0/(\gamma\, 1\,\text{fm})$, where $2r_0$ is the average separation between two nucleons in the rest frame of the nucleus (see Fig. 9). Thus, one can introduce an effective mass number

$$A_{\text{eff}} = \frac{\gamma \Delta z}{2 r_0} \tag{28}$$

and an effective nuclear density along the beam axis,

$$\rho_{\text{eff}} = \frac{3}{2} \frac{A_{\text{eff}}}{\Delta z \, \pi r_0^2} = \frac{\gamma}{4\pi r_0^3/3} = \gamma \, \rho_0 \ , \tag{29}$$

where $\gamma = P/M_N$ is the Lorentz factor of a nucleon in the c.m.$_{NN}$ frame and ρ_0 is the normal nuclear density. The factor $3/2$ accounts for the fact that the density in the middle of the compressed nucleus is larger than on the edges, rather than being homogeneous. This formula is valid only for asymptotically heavy nuclei, because it assumes that the contracted nucleons to fill the entire range $\Delta z = 1$ fm, which for example, would imply for $P = 100$ GeV a mass number $A = (\gamma/r_0)^3$ 1 fm^3 $\simeq$ 6×10^5. For finite nuclei, one has instead
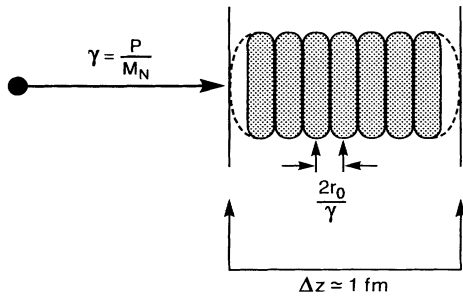

FIG. 9. The incoming proton sees the nucleus in longitudinal direction as a layer of Lorentz contracted nucleons (valence quarks) that are coated by clouds of gluons and sea quarks such that the longitudinal size of the nucleus is about $\Delta z \simeq 1$ fm. The average longitudinal separation between the nucleons however is $2r_0/\gamma$, which is very small compared to Δz for large boosts γ.

$$\rho_{\text{eff}}(A) = \gamma \, \rho_0 \left(\frac{2R_A/\gamma}{\Delta z} \right) = \frac{2r_0 \, \rho_0}{\Delta z} A^{1/3} \tag{30}$$

which increases as $A^{1/3}$, but must approach $\gamma\rho_0$ =const. for $A \to \infty$ and fixed energy. Consequently, for the partons in the incident proton the nucleus appears as a disc with scattering centers (the nuclear partons) that define an effective interaction area $\pi\langle \hat{b}^2\rangle\rho_{\text{eff}}/\Delta z \simeq 1$. Therefore

$$\langle \hat{b}^2 \rangle = \frac{\Delta z}{\pi} \frac{1}{\rho_{\text{eff}}(A)} \propto A^{-1/3} \ , \tag{31}$$

which implies $\langle \hat{b} \rangle \propto A^{-1/6}$.

The essence of the results of Figs. 7 and 8 is that the screening mechanism explained before indeed cuts off scattering at impact parameters $\hat{b} < \hat{b}^{\text{max}}$ which is determined by the parton dynamics. Thus $\langle \hat{b} \rangle$ can be associated with a screening length. In plasma physics the natural regularization of Coulomb-type infrared divergence is provided by the Debye screening length λ^D [45]. Therefore an identification of $\langle \hat{b} \rangle$ with λ^D appears to be plausible. However, the simple screening mechanism developed here, is a concept that is valid for any high density sytem, i.e., no assumptions about specific matter properties, in particular about thermal or chemical equilibrium are necessary. Nevertheless it is satisfactory that the extracted values of $\langle \hat{b} \rangle$ coincide approximately with results for the Debye screening length λ^D in a quark-gluon plasma [46] formed in heavy ion collisions at RHIC and at LHC with typical values $\lambda^D \simeq 0.39$ (0.13) fm at $P = 100$ (3000) GeV [49].

IV. HADRONIC OBSERVABLES

The results that I will present in the following were obtained by hadronizing the final parton configuration at time $t = 3$ fm in the c.m.$_{NN}$ frame, after the initial contact of proton and nucleus, by using the cluster hadronization scheme described in Ref. [5]. I calculated the spectra of hadrons produced in pA collisions for the beam energies and nuclei considered before, namely at $P = 100$ GeV and $P = 3000$ GeV for $p+p$ up to $p+^{238}$U. It was averaged over impact parameters $0 \le b \le \pi R_A^2$. In the c.m.$_{NN}$ frame the partons of the initial proton and nucleus are smeared out around rapidities $y_p = +5.3$ (+8.7) and $y_A = -5.3$ (−8.7) for $P = 100$ (3000) GeV, respectively. What is usually termed "mid-rapidity" is the central region around $y = 0$. The hadronization model is based on a recombination of the final state partons to color neutral clusters that independently fragment and form hadronic states. The secondary partons in the central rapidity region form the "central" clusters that result essentially in a pionization, whereas the spectator partons that have not participated in any interactions, are reassembled to form "beam" clusters giving the leading hadrons and containing most of the baryon number. This phenomenological hadronization is completely independent from the preceding parton cascade evolution in the sense that it may be replaced by any other

suitable hadronization pattern. The cluster hadronization used here has been shown [5] to reproduce a broad range of experimental data on hadron production in e^+e^- annihilation and $p\bar{p}$ collisions at collider energies. The main assumption is the universality of the hadronization mechanism, i.e., that it should be independent of the specific reaction. However, in pA and AA collisions it remains an open question, how medium and nuclear effects may modify the formation of asymptotic hadron states in dense matter. This concerns particularly the particles emerging from the nucleus fragmentation region, which—in the rest frame of the nucleus—are formed inside and may be subject to rescattering and hadronic cascading. These effects are not included in the PCM. Instead, once a hadron is formed, it propagates freely and follows a decay chain to yield its asymptotic state. Because this picture is most likely to be justified in the central rapidity region, where the hadrons are formed after the leading projectile and nuclear remnants have escaped, I will focus on the "pionization" region around zero rapidity.

A. Multiplicities and rapidity spectra

Let me now turn to the question of how the properties of parton interactions discussed in the preceding Secs. II and III might affect hadronic observables. Already in the pre-QCD days of the "naive" parton model [25,27,28] it has been realized that high energy pA collisions can be used as a good probe for the space-time structure of the underlying microscopic parton dynamics. The qualitative picture sketched in Sec. II A and Fig. 1, in which the colliding proton and nucleus are viewed as strongly contracted pancakes of valence quarks surrounded by clouds of virtual gluons and sea quarks, suggests that this property should be reflected by two characteristic rapidity domains observable in the inclusive spectra of secondary hadrons [28], namely $y > y_0$ and $y < y_0$, where $y_0 = y_A + 2.4 \ln A + 1.7$ [39] and $y_A = -5.3$ (-8.7) is the nuclear beam rapidity at $P = 100$ (3000) GeV. The region with $y > y_0$ characterizes the domain where partons of the initial proton that penetrate the nucleus are excited by the layer of gluons and sea quarks around the contracted nucleons (valence quarks) of the nucleus, in the same way as they would be excited were there a single nucleon instead of the nucleus. The nucleus acts as a coherent target and therefore the spectrum of leading particles from the projectile fragmentation should be the same as in a nucleon-nucleon collision. The region with $y < y_0$, on the other hand, is dominated by the excitation of the slow partons of the nucleus due to the penetration of the proton. These excited partons are subject to rescattering and cascading due to the presence of the surrounding nuclear matter. Thus, there should be an enhancement in the multiplicity of formed hadrons when compared to nucleon-nucleon collisions. Such a two-domain structure in the inclusive rapidity spectra is indeed observed at currently achievable beam energies [1]. However at RHIC, and even more at LHC, where the beam energies for pA collisions are by orders of magnitude larger, the spectra might look rather different, as I will discuss now.

The dependence of the multiplicities of produced charged particles on the rapidity variable y and the nuclear mass number A is exhibited in Figs. 10 and 11 for $P = 100$ GeV and $P = 3000$ GeV, respectively. In Fig. 10 the A dependence of the rapidity density dN_{pA}^{ch}/dy of charged hadrons in the central region around $y = 0$ is plotted. The solid lines with full circles display the results of the calculations including the effects of parton saturation and dynamical screening discussed before, whereas the dashed lines with open circles display the neglect of these effects. In Fig. 11 the rapidity spectrum in $p + {}^{197}\mathrm{Au}$ collisions is shown. The main observations from these plots are:

(i) The multiplicity of secondary hadrons with $|y| < 2$ (more than 80% percent of which are pions) shows for light nuclei a strong increase $\sim A^{0.62}$ ($A^{0.65}$), but for $A \gtrsim 40$ the multiplicity growth becomes progressively slower, tending to a $\sim A^{0.33}$ ($A^{0.15}$) behavior for $P = 100$ (3000) GeV. The comparison between the full and dashed curves shows that parton saturation and screening effects significantly reduce the particle production the more the heavier the nuclei. For ${}^{238}\mathrm{U}$ the relative suppression is about 15 (20)%, and for very heavy nuclei ($A \gtrsim 200$) the multiplicity growth around $y = 0$ clearly saturates.

(ii) The height of the prominent peak in the central rapidity region implies a substantial enhancement of particle production in $p + {}^{197}\mathrm{Au}$ collisions by a factor of $\simeq 6.5$ (7.5) as compared to pp collisions at the same $P = 100$ (3000) GeV. In the projectile region $y \gtrsim 4$ (6), the ratio $R^{ch} \simeq 1$, i.e., the spectrum is similar as in pp collisions. In the nucleus fragmentation region $y \lesssim -3$ (-5) there is only a comparably small multiplicity increase due to the breakup of the excited nucleus.

The observation (i) deviates clearly from the common expectation that the cross section for particle production in pA collisions can be represented by a power dependence

$$E \frac{d\sigma_{pA_1}}{d^3p} = \left(\frac{A_1}{A_2}\right)^\alpha E \frac{d\sigma_{pA_2}}{d^3p} , \tag{32}$$
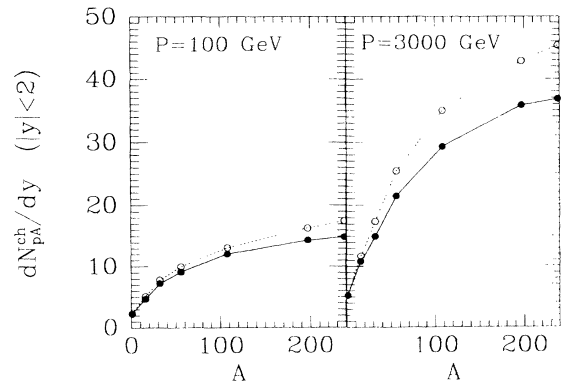

FIG. 10. Rapidity density dN_{pA}^{ch}/dy of charged hadrons in the central region around $y = 0$ vs mass number A in pA collisions at $P = 100$ and $P = 3000$ GeV. The curves full circles include the effects of parton saturation and dynamical screening, whereas the curves with open circles result from neglecting these effects.
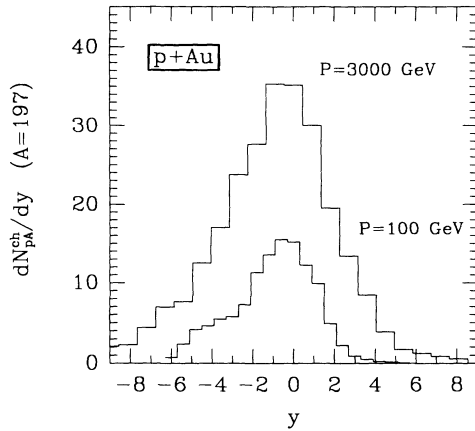
FIG. 11. Rapidity dependence of the ratio (32) of the inclusive charged hadron spectra in pA to pp collisions at the same energies corresponding to $P = 100$ (3000) GeV.

with a parameter $\alpha \equiv \alpha(y, p_\perp)$ that is *independent* of A. For theoretical analyses it is convenient to write

$$\alpha = \frac{2}{3} + \delta , \qquad (33)$$

where the 2/3 is of purely geometric origin, arising from integration over impact parameters, and $\delta \equiv \delta(y, p_\perp)$ parametrizes the nuclear medium effects. For a simple superposition of independent collisions between projectile and the nucleons in the nucleus one would have $\delta = 1/3$, whereas $\delta > 1/3$ ($\delta < 1/3$) reflects the amount of rescattering (shadowing). The form (32) implies for the ratio of multiplicities

$$R^{ch}_{A_1 A_2}(y) = \frac{dN^{ch}_{pA_1}/dy}{dN^{ch}_{pA_2}/dy} = \left(\frac{A_1}{A_2}\right)^\delta . \qquad (34)$$

The parametrization (32) or (34) with an A-independent α or δ fit experimental data astonishingly well over large A ranges and for very different experiments. In contrast to such a simple behavior, Fig. 10 shows a nontrivial A-dependence which corresponds to a decreasing δ as the nuclear size is increased: from $\delta \simeq 0.62$ (0.65) for $A \lesssim 40$ down to $\delta \simeq 0.33$ (0.15) for $A \gtrsim 200$. The reason for this is twofold. First I note that included in the calculations [5] are a number of effects as, e.g., parton shadowing in the initial nuclear structure functions, the Landau-Pomeranchuk-Migdal effect, interfering low-energy gluons, etc., which generally suppress the production of slow partons in parton cascades as the the local density increases with A and with beam energy, or P. Second, with increasing nuclear size, the growing importance of parton fusions and screening effects, as discussed in Sec. III, results in an additional suppression of particle production at small rapidities. For heavy nuclei, the saturation of the parton densities is reflected by a shadowing behavior ($\delta < 1/3$) for the charged particle multiplicity dN^{ch}_{pA}/dy at central rapidity. Therefore it is rather plausible that the intense particle production, characteristic

for collisions with light nuclei due to cascading partons, becomes more and more moderate as A increases.

The property (ii) is elucidated by Fig. 12, where I show again for p+Au the time evolution of the rapidity distributions of secondary partons (those that have interacted at least once). The final parton distributions (full histograms) are the spectra just before hadronization which lead directly to the hadron spectra of Fig. 11. Evidently, particles produced closest to the nuclear beam rapidity y_A, i.e., with $y \lesssim y_A - 3$, result from comparably hard parton collisions at early times $t < 0.5$ fm, involving large $p_\perp^2$ transfers and short time scales $\sim 1/p_\perp$. These are the leading particles, the multiplicity of which is proportional to the volume of the nucleus. With progressing time the presence of the nuclear matter manifests itself in the growing population at smaller rapidities, and shifting towards $y = 0$. The slower secondary partons produced by preceding parton collisions and gluon bremsstrahlung have a large probability to rescatter and to radiate even softer particles. It is interesting to note, that on one hand the typical time scale associated with the softer parton collisions and emission processes increases, so that additional gluon production is suppressed [5] due to the Landau-Pomeranchuk-Migdal effect and soft gluon interference. On the other hand, multiple scattering and parton emission is still effective enough to enhance the population of the central rapidity region compared to pp collisions, as seen from Fig. 11.

At this point I would like to add two remarks.

(1) According to the data analysis of Ref. [1] of multiplicities of produced particles in pA collisions at much lower energy, the multiplicity growth with A is, when parametrized as $dN^{pA}_{ch}/dy = A^\alpha dN^{pp}_{ch}/dy$, obtained as
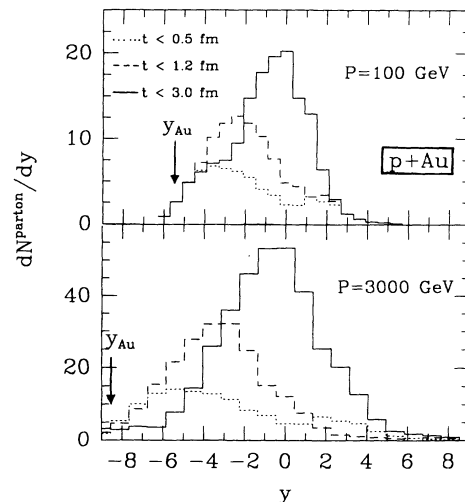

FIG. 12. Time evolution of the rapidity distributions of secondary partons in p+Au. The three histograms in each plot refer to the accumulated multiplicities up to $t < 0.5$ fm (dotted), $t < 1.2$ (dashed), and $t < 3$ fm (solid). The final parton distributions (solid histograms) are the spectra just before hadronization which lead to the charged hadron spectra of Fig. 11.

$\alpha \simeq 0.7$ at central values of the center-of-mass rapidity of the pA system. Compared with this value, the calculated A-dependence in the paper is consistent for light nuclei with $\alpha = 0.65$, however, it progressively deviates by tending to smaller values for heavier nuclei. Thus in the calculations there is no trivial A^α scaling with a constant α, as it is usually assumed. This effect may be interpreted as follows: at current energies I believe one is in the regime where the nuclei in pA collisions in terms of their partonic content appear still rather dilute. This situation corresponds to the lightest nuclei in the PCM at collider energies. These systems are in a sense not too different from pp and therefore the approximate agreement for the α-dependence between experiment and PCM is plausible. However, the heavier the nuclei, the more essential becomes the parton multiplication due to intensified parton cascading which increases the local density very fast to high values so that density effects effectively lead to a suppression of additional particle production. Thus for heavy nuclei the multiplicity increase is considerably slowed down due to dense medium effects.

(2) In confronting Figs. 11 and 12, it becomes evident that there is a direct correlation between the rapidity and the longitudinal space-time evolution [28]. On the one hand the variable y measures the longitudinal extent Δz of the system, since due to Lorentz contraction, Δz is the smaller, the larger y is (cf. Sec. II A). On the other hand, particles with large rapidity emerge from the very early stage ($t \lesssim 0.5$ fm) of the reaction, while particles in the central region at small rapidities are produced during the later stages. Thus, by measuring the rapidity spectra of produced secondary hadrons, one may not only probe the density of the nuclear medium, but also obtain information about the collision dynamics in space-time.

B. Average transverse momentum, transverse energy, and inelasticity

In hadron-nucleus collisions the increase with A of the average transverse momentum per secondary hadron is usually estimated [1] by considering that each additional nucleon of the nucleus that is struck and broken up adds some transverse momentum to the accumulation of $\langle p_\perp^2 \rangle$. Therefore if $\langle p_\perp^2 \rangle \sim \nu$ (ν the average number of struck nucleons), and $\nu \sim A^{1/3}$, as observed in pA collisions at lower energies, one would find that $\langle p_\perp^2 \rangle \sim A^{1/3}$. This picture translates on the parton level to the evolution of parton cascades in which each additional parton collision, emission, or fusion, produces a small transverse momentum kick that accumulates in the average $\langle p_\perp^2 \rangle$ and leads to a diffusion in $p_\perp$ space [14,27]. Intuitively one would guess, that for multiple independent collisions in the absence of collective effects, $\langle p_\perp^2 \rangle$ would scale with the nuclear radius $\propto A^{1/3}$, or $\langle p_\perp \rangle \propto A^{1/6}$. Looking at Fig. 13, where the calculated average $\langle p_\perp \rangle^{ch}$ per secondary charged hadron is plotted versus A, one can extract:

(i) The average $\langle p_\perp \rangle^{ch}$ per particle increases $\propto A^\alpha$ with $\alpha = 0.11$ (0.18) for $P = 100$ (3000) GeV which is close to a $A^{1/6}$ scaling. This growth pattern is however nontrivial. It is strongly correlated with the amount of particle
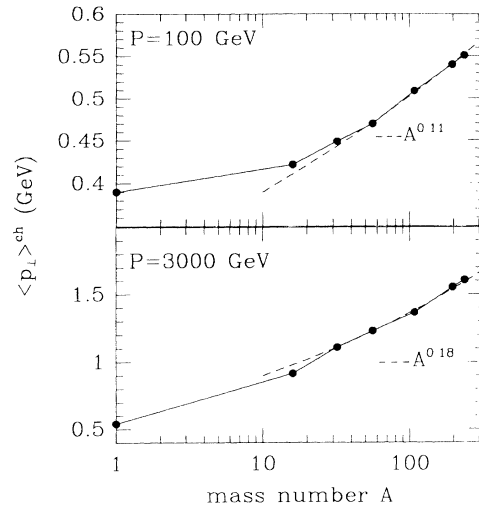

FIG. 13. Nuclear dependence on the mass number A of the calculated average $\langle p_\perp \rangle^{ch}$ per secondary charged hadron in pA collisions at $P = 100$ GeV and $P = 3000$ GeV.

production by cascading partons. The latter increases the slower with A the heavier the nucleus (Sec. IV A), so that for a fixed amount of total transverse momentum produced, the average $\langle p_\perp \rangle^{ch}$ per particle is enhanced.

I would like to add a comment with regard to current experimental knowledge of high-energy pA collisions at the FNAL accelerator. The A dependence of $\langle p_\perp \rangle^{ch}$ is consistent with the measurements of the parton-parton dijet cross section in the Fermilab experiments on proton-nucleus collisions with $p_{\text{Lab}} = 400$ GeV [51] and $p_{\text{Lab}} = 800$ GeV [52] proton momentum incident on the nucleus at rest. A comparison with the data may be a bit far fetched, because these beam momenta are orders of magnitude smaller than the collider energies considered in the calculations here (cf. Table I). Nevertheless it is worth mentioning that in the experiments the average transverse momentum per outgoing parton was observed (extracted from the hadron spectra by means of a jet finding algorithm) to increase as A^α with $\alpha = 0.11 - 0.16$ which indicates that there is indeed substantial secondary scattering of partons by nuclear matter even at these much smaller beam energies than will be available at the RHIC or LHC.

Another interesting question is, how much of the initial total energy of the pA system is harnessed in producing secondary particles and how much of the longitudinal beam momentum is degraded. Two direct observables that measure the violence of the reaction are the total transverse energy of secondary particles $E_\perp$ [53] and the inelasticity I or thrust $T = 1 - I$ [54]. The transverse energy measures the amount of energy redirected in transverse direction and may also serve as an indicator of the energy density achieved. It is defined as

$$E_\perp = \sum_i p_{\perp i} \sqrt{1 + \frac{m_i^2}{p_i^2}} , \qquad (35)$$

where the sum is understood to count exclusively contributions from secondary particles, $p_{\perp i} = |\mathbf{p}_{\perp i}|$ is the transverse momentum of particle i perpendicular to the beam axis, m_i its rest mass, and $p_i = |\mathbf{p}_i|$ labels here the magnitude of three momentum. The quantity thrust on the other hand, exhibits to which degree the initial longitudinal momentum of proton and of the nucleus is degraded (nuclear stopping power) by measuring the fraction of left over longitudinal momentum carried by the spectator particles,

$$T = \frac{\sum_i |p_{zi}|_{\text{spec}}}{\sum_i |\mathbf{p}_i|} . \tag{36}$$

Here $p_{z\,i}$ is the longitudinal momentum of the ith particle with respect to the beam axis and the sum in the numerator runs only over those particles that remained spectators, whereas the denominator is the total three-momentum of all particles. Note that initially, before the collision, T is close to unity because the small primordial transverse momentum and Fermi motion is negligible compared to the large beam momentum P. During the collision the longitudinal momentum of interacting partons is converted in transverse direction and at the same time the number of spectators is reduced, whereas the total three-momentum is conserved. At the end of the parton evolution the drop of T indicates the inelasticity on the parton level. The subsequent hadronization further reduces T only by a negligible amount, so that the inelasticity extracted from the hadron spectra can be identified with the partons' dissipation.

In Figs. 14 and 15 the A dependence of the total produced transverse energy per nucleon $E_\perp/A$ and of the thrust T is plotted versus the nuclear mass number A, again for $P = 100$ GeV and $P = 3000$ GeV. The essential observations are consistent with the multiplicity and transverse momentum properties discussed before:

(ii) For small nuclei ($A \lesssim 30$) the increase of $E_\perp/A$ is weak. For intermediate nuclei $30 \lesssim A \lesssim 150$ a comparably
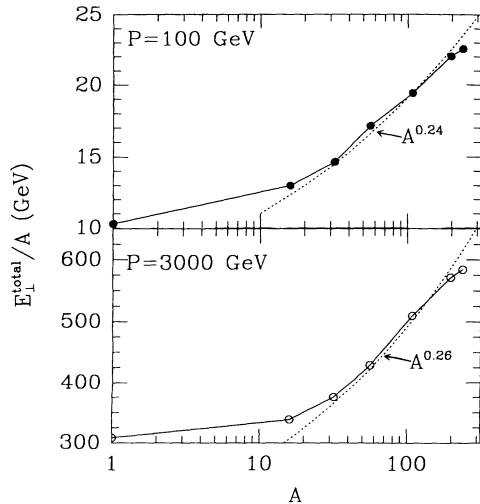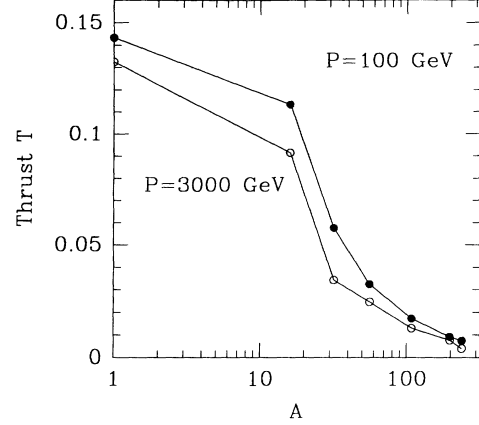

FIG. 15. Nuclear dependence of the thrust T, measuring the effect of inelasticity or nuclear stopping power, in pA collisions at the two considered beam energies corresponding to $P = 100$ (3000) GeV.

strong growth proportional $A^{0.24}$ ($A^{0.26}$) becomes effective, which is close to what is observed for lower energies at the SPS [53]. For heavy nuclei ($A \gtrsim 200$) however, $E_\perp/A$ appears to saturate. This saturating behavior indicates that there is an upper limit for energy deposition which arises because the initial available beam energy is shared by more and more nucleons but the transverse energy per particle does not increase further.

(iii) The nuclear stopping exhibited by the A dependence of the thrust T repeats the pattern of the transverse energy production. Light nuclei with $A \lesssim 10$ appear almost as transparent as a single nucleon, but then with increasing A the nuclei become rapidly more absorptive. Again there is a clear saturation evident for very heavy nuclei, i.e., $T \to 0$. This is of course expected, since a nucleus cannot be blacker than black, or, in other words, the proton penetrating the nucleus cannot be more than completely stopped.

V. SUMMARY

In this paper I studied how the transport of partons and their interactions in ultrarelativistic nuclear collisions can be affected in the environment of dense nuclear matter. Singling out from the multitude of different nuclear and medium effects, some of which have been discussed earlier, three closely related aspects of QCD in medium: first, the saturation of the parton phase-space densities enforced to unitarity conservation, second, the interplay and balance between emission and fusion processes, and third, the local screening of parton interactions due to the presence of dense quark-gluon matter. Within the framework of the statistical approach of the PCM, I investigated how the kinetic evolution of the parton densities is modified by these effects. As a realistic scenario, proton-nucleus collisions at beam energies typical for the future collider experiments at the RHIC and the LHC were considered. These reactions provide rather well-defined initial conditions and allow one to use the

FIG. 14. A-dependence of the total produced transverse energy per nucleon $E_\perp/A$, again for $P = 100$ GeV and $P = 3000$ GeV.

proton as a probe of the space-time evolution. The dependence on the nuclear size and beam energy can be studied without additional complexities arising from a QCD phase transition and a quark-gluon plasma formation expected in heavy ion collisions. Two beam energies corresponding to $P = 100$ GeV and $P = 3000$ GeV beam momentum per nucleon and various nuclei covering the full range $A = 1 \ldots 238$ were considered.

The conclusions for the evolution of partons in these reactions are as follows:

(i) The unitarity principle enforces an upper limit on gluon production and imposes a maximum parton density which is controlled by the balance of emission and fusion processes. The unitarity limit is almost reached already for $P = 100$ GeV in $p + {}^{238}$U collisions at central rapidity and it is fully reached at $P = 3000$ GeV for nuclei $A \gtrsim 200$ GeV. The time scale associated with approaching the maximum density is ≈ 2 fm at $P = 100$ GeV and roughly twice as fast for $P = 3000$ GeV. For proton on light nuclei, the parton densities remain—at the considered beam energies—well below the saturation limit.

(ii) In the statistical picture of parton evolution the self-contained balance between gluon emission by excited cascading partons and parton-parton fusion results in a rapid stabilization of the average transverse momentum of interacting partons. As a consequence the parton cross section becomes peaked at a characteristic value $p_{\perp 0}$ that depends on both the beam energy and the nuclear size. Below and above this value the cross section is strongly damped, so that it is rendered finite over the full kinematic range.

(iii) A simple mechanism for the screening of parton interactions in medium has been implemented that is governed by the dynamical evolution. The screening is provided by the space-time dependent phase-space occupation and accomplishes a self-consistent regularization of the infrared singularity of the effective parton cross section. Long range interactions corresponding to large impact parameters of partons are naturally cut off provided the surrounding matter is sufficiently dense. For beam energies at RHIC and LHC this condition is already satisfied in pA collisions with $A \gtrsim 30$ GeV. The extracted typical screening length is comparable to estimates based on thermal QCD calculations. This demonstrates that it is possible to include soft interactions (usually classified as "nonperturbative" and treated phenomenologically) in the framework of the perturbative QCD evolution.

The consequences for experimental observables in the properties of produced hadrons are found as:

(iv) The particle production in the central rapidity regions is the overwhelming source of entropy even in pA reactions and results in an intense pionization. In the nuclear fragmentation region the number of produced hadrons is comparably small, because the nucleus is almost completely broken up, with most of its fragments considerably slowed down and shifted towards central rapidity. Contrary to common expectation, there is no simple A^δ power dependence with a constant δ in the multiplicity increase with A observed. Instead a strong growth with $\delta \simeq 0.6$ for light nuclei merges in a shad-

owing behavior with $\delta \lesssim 1/3$ for the heaviest nuclei. The dependence on the beam energy of dN/dy is estimated to come close to $\propto (\ln P)^2$ rather than linear in $\ln P$ [55].

(v) The average transverse momentum per secondary hadron scales roughly as $A^{1/6}$, reflecting the substantial amount of multiple scattering and cascading on the parton level that results in a diffusion-type spread of transverse momentum. The dependence on the initial beam momentum P for fixed A is approximately $\langle p_\perp \rangle \propto \ln P$ which is consistent with the expectation that the increase of transverse momentum is approximately related to the growth of central multiplicity as $\langle p_\perp \rangle \propto \sqrt{dN/dy}$.

(vi) The amount of total produced transverse energy is not too far from a $A^{1/3}$-scaling for nuclei with $A \gtrsim 30$ up to $A \approx 150$, beyond which a saturation of $E_\perp/A$ is found due to a maximum energy deposition for fixed initial beam energy. Related to this behavior is the strong increase of nuclear stopping power with increasing nuclear size that is reflected by the magnitude of inelasticity or thrust. Again, for the heaviest nuclei the further growth of inelasticity (decrease of thrust) tends to stop as the projectile proton is completely absorbed and stopped by the nucleus.

In summary, I would like to stress that although the present analysis does not indicate any spectacular new physics to be expected with the advent of RHIC and LHC, it showed that it is very important to study and understand in detail, both theoretically and experimentally, the various nuclear and medium effects and their possible interference. The very well founded framework of improved QCD perturbation theory for semihard processes provides a good basis for more accurate predictions once these medium effects are better understood. In fact, one can expect that "QCD in medium" will resolve the problems associated with infrared divergent behavior of "QCD in vacuum." Aside from this task it is of great importance to establish a rigorous quantum kinetic theory on the basis of Wigner functions rather than classical phase-space densities. By relating the experimentally accessible parton number densities of the nucleon structure functions with the Wigner functions in full phase-space, a connection between the Altarelli-Parisi-Lipatov evolution equations in momentum space and the Boltzmann equation in space-time must be established. The semiclassical PCM approach serves here as a pragmatic first step, but ultimately a space-time description well founded on the principles of quantum field theory is desired.

ACKNOWLEDGMENTS

[1] S. Fredriksson *et al.*, Phys. Rep. **144**, 187 (1987); J. Rutherfoord, in *Intersections Between Particle and Nuclear Physics, Proceedings of the Third Conference, Rockport, MA, 1988*, edited by G. Bunce, AIP Conf. Proc. No. 176 (AIP, New York, 1988).

[2] B. Müller, in *Particle Production in Highly Excited Matter*, edited by H. Gutbrod and J. Rafelski (Plenum, New York, 1993); *Quark Gluon Plasma*, edited by R. C. Hwa (World Scientific, Singapore, 1990).

[3] For a recent overview on the status of high energy nucleus-nucleus collisions, see *Quark Matter '91*, Proceedings of the Ninth International Conference on Ultrarelativistic Nucleus-Nucleus Collisions, Gatlinburg, Tennessee, 1991, edited by T. C. Awes *et al.* [Nucl. Phys. **A544**, 1c (1992)].

[4] K. Geiger and B. Müller, Nucl. Phys. **B369**, 600 (1992).

[5] K. Geiger, Phys. Rev. D **47**, 133 (1993).

[6] K. Geiger, Phys. Rev. D **46**, 4986 (1992); K. Geiger and J. I. Kapusta, Phys. Rev. Lett. **70**, 1290 (1993); K. Geiger, Phys. Rev. Lett. **71**, 3075 (1993); K. Geiger and J. I. Kapusta, Phys. Rev. D **47**, 4905 (1993); K. Geiger, Phys. Rev. D **48**, 4129 (1993).

[7] The maximum achievable beam energy and the luminosity at RHIC and LHC actually depend on the reaction. The concept of a collider accelerator with bunched beams requires that for pA and for AA experiments both beams have the same Lorentz factor, but the maximum energy is set by the nucleus and varies with its size. For instance at RHIC, the highest center-of-mass energy per nucleon pair varies from 250 GeV for oxygen down to 200 GeV for gold nuclei.

[8] UA5 Collaboration, Phys. Rep. **154**, 247 (1987).

[9] X. N. Wang, Phys. Rev. D **43**, 104 (1991); X. N. Wang and M. Gyulassy, Phys. Rev. D **44**, 3501 (1991).

[10] K. Hahn and J. Ranft, Phys. Rev. D **41**, 1463 (1991); P. Aurenche *et al.*, Phys. Rev. D **45**, 92 (1992).

[11] Proceedings of the Workshop on Pre-equilibrium Parton Dynamics in Heavy Ion Collisions, LBL-Report 34831, 1993 (unpublished).

[12] Klaus Geiger, Nucl. Phys. **A566**, 257c (1994).

[13] L. V. Gribov, E. M. Levin, and M. G. Ryskin, Phys. Rep. **100**, 1 (1983).

[14] E. M. Levin and M. G. Ryskin, Phys. Rep. **189**, 267 (1990).

[15] K. Kajantie, P. V. Landshoff, and J. Lindfors, Phys. Rev. Lett. **59**, 2527 (1987).

[16] R. C. Hwa and K. Kajantie, Phys. Rev. Lett. **56**, 696 (1986).

[17] J.-P. Blaizot and A. H. Mueller, Nucl. Phys. **B289**, 847 (1987).

[18] A. H. Mueller, Nucl. Phys. **A498**, 41c (1989).

[19] K. J. Eskola, K. Kajantie, and J. Lindfors, Nucl. Phys. **B323**, 37 (1989).

[20] X.-N. Wang, Phys. Rev. D **43**, 104 (1990); X.-N. Wang and M. Gyulassy, Phys. Rev. Lett. **68**, 1480 (1992).

[21] K. Eskola and X.-N. Wang, "Space-time Structure of Initial Parton Production in Ultra-relativistic Heavy Ion Collisions," Report No. LBL-34156 UC-413, 1993 (unpublished).

[22] M. Gyulassy and X.-N. Wang, "Multiple Collisions and Induced Gluon Radiation in QCD," Report No. LBL-32682 UC-413, 1993 (unpublished).

[23] A. Selikov and M. Gyulassy, "Color Diffusion and Color Conductivity," Report No. CU-TP-598A, 1993 (unpublished).

[24] E. V. Shuryak, Phys. Rev. Lett. **68**, 3270 (1992); E. V. Shuryak and L. Xiong, Phys. Rev. Lett. **70**, 2241 (1993); "Gluon Multiplication in High Energy Heavy Ion Collisions," Report No. SUNY-NTG-93-24, 1993 (unpublished).

[25] R. P. Feynman, *Photon Hadron Interactions* (Benjamin, New York, 1972).

[26] V. N. Gribov, in Proceedings of the VIII LNPI Winter School, Leningrad, 1973, Vol. 2.

[27] J. Kogut and L. Susskind, Phys. Rep. **8**, 75 (1973).

[28] J. D. Bjorken, in *Proceedings of the International Summer Institute on Theoretical Particle Physics, Hamburg, 1975*, edited by J. Körner *et al.*, Lecture Notes in Physics Vol. 56 (Springer, New York, 1976).

[29] G. Reya, Phys. Rep. **69**, 195 (1981).

[30] A. H. Mueller Phys. Rep. **73**, 237 (1981).

[31] G. Altarelli, Phys. Rep. **81**, 1 (1982).

[32] A. Bassetto, M. Ciafaloni, and G. Marchesini, Phys. Rep. **100**, 203 (1983).

[33] *Perturbative Quantum Chromodynamics, Advanced Series on Directions in High Energy Physics*, edited by A. H. Mueller (World Scientific, Singapore, 1989), Vol. 5.

[34] 1989 RHIC Conceptual Design Report, BNL publication 52195, 1989.

[35] J. Schukraft, talk given at the Workshop on a dedicated Heavy Ion Detector for LHC, CERN, Feb. 1993.

[36] K. Geiger, Phys. Rev. D **46**, 4965 (1992).

[37] See, e.g.: H.-Th. Elze and U. Heinz, Phys. Rep. **183**, 81 (1989); S. Mrówczyński, Phys. Rev. D **39**, 1940 (1989).

[38] N. Abou-El-Naga, K. Geiger, and B. Müller, J. Phys. G **18**, 797 (1992).

[39] E. M. Levin and M. G. Ryskin, Nucl. Phys. **B304**, 805 (1989).

[40] A. Mueller and J. Qiu, Nucl. Phys. **B286**, 427 (1986).

[41] K. Henzi and P. Valin, Phys. Lett. **160B**, 167 (1985).

[42] L. Durand and H. Pi, Phys. Rev. Lett. **58**, 303 (1987).

[43] X.-N. Wang, Phys. Rev. D **43**, 104 (1991).

[44] R. Cutler and D. Sivers, Phys. Rev. D **17**, 196 (1978); B. L. Combridge, Nucl. Phys. **B151**, 429 (1979); P. Nason, S. Dawson, and R. K. Ellis, Nucl. Phys. **B303**, 607 (1988); **B327**, 49 (1989); **B335**, 260 (1990).

[45] See, for example, R. Balescu, *Statistical Mechanics of Charged Particles* (Interscience, London, 1963).

[46] E. Shuryak, Zh. Eksp. Teor. Fiz. **74**, 408 (1978) [Sov. Phys. JETP **47**, 212 (1978)]; M. B. Kislinger and P. D. Morley, Phys. Rep. **51**, 63 (1979); H. A. Weldon, Phys. Rev. D **26**, 1394 (1982).

[47] Taking $\Delta t = 10^{-2}$ fm implies that the outgoing states c and d in a parton scattering $ab \to cd$ are not asymptotic states after such a short time, in the sense as used in the parton-parton cross sections. The question is, how long after a scattering does it take until a parton can be considered an approximate asymptotic state. This is currently described in the PCM in a crude way [36] by taking into account for each interaction the characteristic time scale, given by the uncertainty relation, for the production of the outgoing particles as truly resolvable quanta.

[48] Actually a more general procedure is realized in the PCM by employing a normalized probability distribution $\Phi(b/b^{\max})$ which a less rigid cutoff than $\Phi(b/b^{\max}) = \Theta(1-b/b^{\max})$ which corresponds to Eq. (23). A rather diffuse distribution appears to be more appropriate, since

the cross-section $\hat{\sigma}_{ab}$ is generally dominated by small-angle scatterings, corresponding to large impact parameters. The particular choice employed is $\Phi(b/b^{max}) = \exp(-b/b^{max})$ which requires, instead of Eq. (23), $b < b^{max}\ln(R)$, where R is a uniform random number between 0 and 1.

[49] B. Müller and X.-N. Wang, Phys. Lett. B **283**, 171 (1992); S. Mrówczyński, Phys. Lett. B **314**, 118 (1993); "Color Collective Effects at the Early Stage of Ultrarelativistic Heavy Ion Collisions," report, 1993 (unpublished).

[50] M. Kalelkar, in *Hadronic Matter in Collision*, edited by P. Carruthers and J. Rafelski (World Scientific, Singapore, 1989).

[51] T. Fields, Nucl. Phys. **A544**, 565c (1992); M. D. Corcoran *et al.*, Phys. Lett. B **259**, 209 (1991).

[52] C. Stewart *et al.*, Phys. Rev. D **42**, 1385 (1990).

[53] M. Tindell, in *Hadronic Matter in Collision*, edited by P. Carruthers and J. Rafelski (World Scientific, Singapore, 1989); M. Tannenbaum, Int. J. Mod. Phys. A **14**, 3377 (1989).

[54] J. D. Bjorken and S. J. Brodsky, Phys. Rev. D **1**, 1416 (1970).
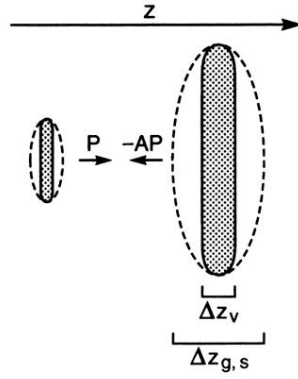
[55] F. Abe *et al.*, Phys. Rev. D **41**, 2330 (1990).

FIG. 1. Illustration of the "Lorentz distributed contraction" of proton and nucleus in the c.m.$_{NN}$ frame. The incident proton sees the nucleus as several layers of highly Lorentz contracted nucleons that are surrounded by a cloud of virtual gluons and sea quarks.
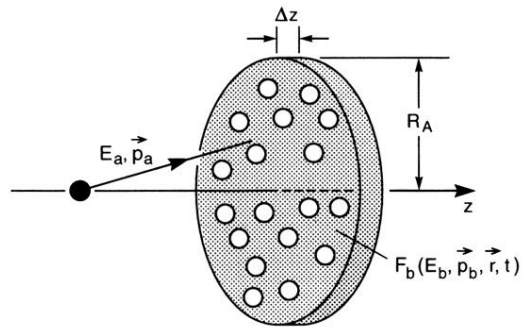
FIG. 3. A parton a under consideration can interact during a time span Δt with all kinds of partons b, that are contained in the volume $\Delta z \pi R_A^2$ which the parton a traverses within Δt. The density of scatterers F_b determines the magnitude of the interaction probability W_a.
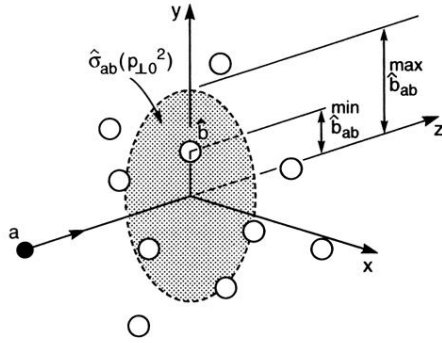
FIG. 6. Illustration of the prescription for choosing for a given parton a the collision partner b. Of all potential scattering candidates b contained within the effective interaction area $\pi(\hat{b}_{ab}^{max})^2$, given by the cross section $\hat{\sigma}_{ab}(p_{\perp 0}^2)$, the one with the minimum impact parameter $\hat{b}_{ab}^{min}$ is selected.
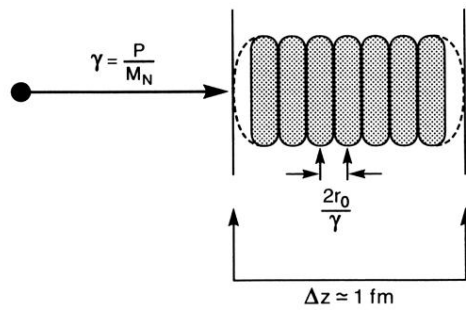
FIG. 9. The incoming proton sees the nucleus in longitudinal direction as a layer of Lorentz contracted nucleons (valence quarks) that are coated by clouds of gluons and sea quarks such that the longitudinal size of the nucleus is about $\Delta z \simeq 1$ fm. The average longitudinal separation between the nucleons however is $2r_0/\gamma$, which is very small compared to Δz for large boosts γ.